DAA/ [illegible]
NAG1-394

Department of

Mechanical and Aerospace Engineering

IN-71
63692
61P

NASA Grant NAG 1-394

A COMPARISON OF THE STRUCTUREBORNE AND AIRBORNE PATHS FOR PROPFAN INTERIOR NOISE

Final Report

W. Eversman, L. R. Koval, J. V. Ramakrishnan

(NASA-CR-180289) A COMPARISON OF THE STRUCTUREBORNE AND AIRBORNE PATHS FOR PROPFAN INTERIOR NOISE Final Report (Missouri Univ.) 61 p Avail: NTIS HC A04/MF A01 CSCL 20A G3/71
N87-26612
Unclas
0063692

University of Missouri-Rolla

NASA Grant NAG 1-394

A COMPARISON OF THE STRUCTUREBORNE AND AIRBORNE PATHS FOR PROPFAN INTERIOR NOISE

Final Report

W. Eversman, L. R. Koval, J. V. Ramakrishnan

October 1986

Mechanical and Aerospace Engineering Department
University of Missouri-Rolla
Rolla, MO 65401

ABSTRACT

A comparison is made between the relative levels of aircraft interior noise related to structureborne and airborne paths for the same propeller source. A simple, but physically meaningful, model of the structure treats the fuselage interior as a rectangular cavity with five rigid walls. The sixth wall, the fuselage sidewall, is a stiffened panel. The wing is modelled as a simple beam carried into the fuselage by a large discrete stiffener representing the carry-through structure. The fuselage interior is represented by analytically-derived acoustic cavity modes and the entire structure is represented by structural modes derived from a finite element model. The noise source for structureborne noise is the unsteady lift generation on the wing due to the rotating trailing vortex system of the propeller. The airborne noise source is the acoustic field created by a propeller model consistent with the vortex representation. Comparisons are made on the basis of interior noise over a range of propeller rotational frequencies at a fixed thrust. The measure of noise level is based on nonresonant response to eliminate the large variations associated with unquantifiable damping levels. It is found that the relative importance of the structural and airborne paths is highly dependent on the structural parameters. Over the range of parameters considered in this study it is found that the structureborne contribution can vary from very insignificant to nearly equivalent to the airborne levels.

INTRODUCTION

The question addressed here is the relative importance of structureborne and airborne paths for propeller noise in aircraft interiors. Of particular interest are wing-mounted engines driving multiple-blade propfans.

A significant design consideration in the installation of advanced propfan propulsion systems on transport category aircraft is the interior noise level within the passenger compartment. The extrapolation of experience gained with conventional propeller-driven aircraft and the current generation of turboprop aircraft indicates that in the case of the advanced, highly loaded, multiple-blade propellers currently proposed the interior noise levels may exceed comfort levels and may even exceed hearing damage levels. It is therefore important to understand not only the noise generating mechanism, but also the paths by which the noise is transmitted into the aircraft interior.

Advanced turbofan engines are likely to be tractor or pusher wing-mounted installations or pusher aft mounted installations. The tractor wing-mounted engine, typical of current turboprop aircraft, has the most significant structure-borne noise implications because of the interaction of the propeller trailing vortex system with the wing structure. It is this configuration which is considered here.

For several years there has been considerable speculation on the relative importance of airborne and structureborne paths for the transmission of propeller noise into the fuselage. The interaction of the propeller rotating trailing vortex system with the wing structure creates an oscillatory forcing function on the wing which can be transmitted into the fuselage interior through the wing and fuselage structural coupling to the cavity. The airborne path describes the mechanism by which the propeller radiated noise field is transmitted through the fuselage sidewall to the fuselage cavity.

No significant data base exists on the relative importance of the structureborne and airborne paths. Measurements to isolate the two sources on an unmodified aircraft are not possible with current experimental methods. Identification of the two sources will probably require physical isolation, for example, breaking the structural path by disconnecting the wing from the fuselage or breaking the airborne path by placing a barrier between the propeller and the fuselage. Tests of this type are major undertakings and have not to date been accomplished to the point of providing useable data.

Very little work has been done on the modelling of the structureborne noise paths. In contrast, fairly extensive models have been developed for airborne noise [for example; 1,2,3]. Metcalf and Mayes [4] addressed the question of the possibility of a significant contribution of structureborne noise to the overall interior noise levels based on tests which broke the airborne noise path by wrapping the fuselage of the test aircraft with an acoustical barrier material. In a related study, Unruh [5] examined the structureborne noise path which transmits engine vibrations in a single engine general aviation aircraft by an experimental technique in which the engine was isolated from the fuselage.

Until recently no substantial attempt has been made to produce an analytical model of the structureborne path for propeller noise. Junger, Garrelick, Martinez and Cole [6] appear to be the first to consider the introduction of propeller wake disturbances into the wing structure and subsequent wave propagation into the fuselage structure. Their model was based on a Green's function approach treating the wing structure as an acoustic wave guide, as discussed by Junger and Feit [7].

In the present study a model is created which can be used to compare structureborne and airborne noise levels in the fuselage cavity. The mechanism for the introduction of propeller noise into the fuselage is basically the same as that used by Junger, Garrelick, Martinez and Cole [6]. The airborne noise source level is also modelled here using a finite element propeller radiation model which predicts the radiated acoustic field of the propeller [8]. This model can be used in the near field of the propeller. For relatively small fuselage-propeller tip clearances the near field is important.

The structural-acoustic system is based on a simple geometry which approximates the essential features of the wing-fuselage structure and the cabin interior. The interior is modelled as a rectangular cavity. The sidewall is modelled as a flat stiffened panel. The wing is modelled as a beam which is carried into the fuselage structure by a heavy discrete stiffener. The wing-fuselage is represented by a finite element procedure from which the free vibration frequencies and normal modes are determined. The cavity is represented in terms of its hardwall acoustic natural frequencies and normal modes. For the rectangular cavity, or for the logical extension to a cylindrical cavity, the acoustic modes can be represented analytically. A coupling procedure discussed by Dowell, Gorman, and Smith [9] is used to construct the complete system model.

The interior noise levels can be calculated in response to the structureborne and airborne noise sources. The approach used here is to consider a particular propeller geometry operating at a fixed thrust and a given forward speed. This fully defines the airborne noise levels and the strength of the propeller vortex system for the structureborne source. The sound pressure level at a reference point in the cavity is calculated for a range of propeller rotational speeds. For a fixed thrust, this means that blade twist and loading are changed. The comparison of interior noise levels is based on the level of the nonresonant response to eliminate uncertainties created by unquantifiable levels of structural damping.

Heitman and Mixson [10] have found that interior acoustic absorption may play an important role in controlling the levels of airborne interior noise.

In the present formulation a model of this type of acoustic treatment has been included. The results of computations including interior absorption will be reported later in this report.

THE MODEL FOR THE STRUCTUREBORNE NOISE SOURCE

The mechanism for the generation of structureborne noise is the interaction of the propeller tip vortex system with the wing. This interaction creates a spanwise variation of lift which varies periodically in time. Figure 1 shows, in simplified form, the trailing vortex system from a two-bladed propeller. The vortex system, created by the lift on the propeller blades, is swept around with the rotating propeller. The velocity field of each vortex modifies the downwash on the wing and, therefore, locally creates a periodic lift variation.

The velocity field behind the propeller is very complicated, but the important features of the interaction with the wing can be modelled by assuming that there is associated with each propeller a vortex, the circulation of which is determined by the lift per unit span at the propeller tip. The bound vorticity on the propeller and the vortex sheet immediately behind the propeller are neglected so that only the fully developed rolled up tip vortex system is considered to be important. This description of the vortex system is consistent with the model of Junger, Garrelick, Martinez, and Cole [6].

The physical picture is that of an isolated vortex trailing from each propeller blade and rotating with the propeller. In an axis system centered on the vortex the induced velocity field is

$$\vec{V} = (\Gamma/2\pi h)\ \vec{e}_t$$

where Γ is the circulation strength of the vortex, h is the distance from the vortex center to the point at which the velocity $\vec{V}$ is calculated, and $\vec{e}_t$ is a unit vector normal to the line between the vortex center and the point at which $\bar{V}$ is calculated (i.e. a unit vector tangent to the circular streamline of the vortex).

With this model it is possible to represent the normal wash on the plane Z = 0 (in which the axis of the propeller lies) in four regions on the wing:

$0 < \eta < 1$: The region behind the propeller disk and outboard of the propeller hub

$$\bar{w} = -\sum_{\ell=1}^{\infty} \eta^{\ell N-1} \cos \ell N \Omega t \tag{1}$$

$\eta > 1$: Outboard of the propeller disk

$$\bar{w} = \sum_{\ell=0}^{\infty} \eta^{-(\ell N+1)} \cos \ell N \Omega t \tag{2}$$

$-1 < \eta < 0$: The region behind the propeller disk and inboard of the propeller hub

$$\bar{w} = \sum_{\ell=1}^{\infty} (-1)^{\ell N+1} |\eta|^{\ell N-1} \cos \ell N \Omega t \tag{3}$$

$\eta < -1$: Inboard of the propeller disk

$$\bar{w} = \sum_{\ell=1}^{\infty} (-1)^{\ell N+1} |\eta|^{-(\ell N-1)} \cos \ell N \Omega t \tag{4}$$

where

$$\eta = (Y-Y_o)/R$$

and

Y_0 = Spanwise location of the propeller axis

Y = Spanwise location of the normal wash point

R = Propeller radius

Ω - Propeller rotational speed (radians/sec.)

N - Number of propeller blades

$\bar{w}$ - Normal wash (positive in the direction of positive z, upward)

and

$$w = (\Gamma/2\pi R)\ \bar{w} \qquad (5)$$

Figure 2 shows the spanwise variation of normal wash amplitude.

The tip vortex strength Γ is determined from the lift per unit span at the tip

$$\ell_t = \rho V \Gamma \qquad (6)$$

where

ℓ_t = lift per unit span at the tip

V = helical velocity at the tip

ρ = air density

The circulation can thus be written as

$$\Gamma = \ell_t / \{\rho U [1 + (\Omega R/U)^2]^{1/2}\} \qquad (7)$$

where U is the forward velocity. The parameter ℓ_t depends on the propeller model used. Junger, Garrelick, Martinez, and Cole [6] use a triangular loading which when combined with a given total lift, number of blades, forward flight dynamic pressure, propeller radius, and rotational speed, will define the entire propeller loading, and in particular, the tip loading. This type of loading is consistent with the actual loading on conventional propellers [11].

The resulting lift per unit span is

$$\ell = (1/2)\ \rho U^2 (1 + J^{-2}) C_t C_{\ell_{\alpha_t}}\ \alpha_t (r/R) \qquad (8)$$

and the resulting thrust loading and torque loading per unit span are

$$t = (1/2)\ U^2 (1 + J^{-2}) C_t C_{\ell_\alpha} \alpha_t (r/R) \cos\beta \qquad (9)$$

$$m = 1/2\ \rho U^2 (1 + J^{-2}) C_t C_{\ell_{\alpha_t}} \alpha_t (r/R) \sin\beta \qquad (10)$$

where the angle β, the angle between the helical velocity and the propeller disk, is defined by

$$\cos\beta = (r/JR)[1 + (r/R)^2 J^{-2}]^{-1/2} \qquad (11)$$

$$\sin\beta = [1 + (r/R)^2 J^{-2}]^{-1/2} \qquad (12)$$

The parameter J is defined by

$$J = U/\Omega R \qquad (13)$$

and is proportional to the advance ratio used in the propeller literature. Also defined here are

C_t = propeller tip chord

α_t = tip angle of attack

$C_{\ell_{\alpha_t}}$ = propeller lift curve slope at the time

The value of the tip angle of attack is determined by the total thrust where

$$T = N\ell_t \frac{R}{2} \left\{[(1 + J^2)^{1/2} - J^2 \ell\eta [J^{-1} + (1 + J^{-2})^{1/2}]\right\} \qquad (14)$$

where

$$\ell_t = (1/2)\ \rho U^2 (1 + J^{-2}) C_t C_{\ell_{\alpha_t}} \alpha_t \qquad (15)$$

Equations (7) and (14) are sufficient to determine Γ, given the propeller thrust, geometry, and rotational speed. Equations (9) and (10) can then be used to compute the propeller loading. The loading is required in the calculation of the airborne sound pressure levels.

The normal wash distribution given by Eqs. (1)-(5) locally creates an effective angle of attack of the wing given by

$$\alpha_w = W/U \qquad (16)$$

which creates a lift force on the wing. In this analysis we use the quasi-static assumption and calculate the lift according to a strip theory representation as

$$\ell_w = (1/2)\ \rho U^2 C_w C_{\ell_{\alpha_t}} \alpha_w \qquad (17)$$

where

$C_{\ell_{\alpha_t}}$ = 2π, the theoretical two dimensional lift curve slope for incompressible, steady flow

ℓ_w = lift per unit

C_w = wing chord

Junger, Garrelick, Martinez, and Cole [6] use a correction for unsteady flow and compressibility. However, this is not considered to be essential in the present analysis since such a refinement is certainly lost in other approximations which are required. Since the lift distribution is directly proportional to the downwash amplitude distribution, it follows that Figure 2 also can be viewed as a distribution of the oscillatory lift distribution on the wing.

An examination of Eqs. (1)-(5) and Eqs. (16) and (17) shows that for a specific propeller rotational speed Ω, the structureborne source frequencies are harmonics of $N\Omega$, where N is the number of propeller blades. These are exactly the harmonics of the airborne noise source. In making computations of interior noise related to the structureborne source it has been found that the interior noise levels are well defined with two or three harmonics being computed.

THE MODEL FOR AIRBORNE NOISE

In order to compare the relative importance of airborne and structural paths for interior noise, it is necessary to have a model for airborne noise which is consistent with the model for the structureborne noise source discussed above. Such a model has been created by Eversman and Steck [8]. In this model the propeller is represented by a thrust loading and torque loading distribution in the propeller disk. The loading which is used is given by Eqs. (9) and (10) and is therefore consistent with the structureborne noise source. The thrust and torque loading become the volumetric force distribution in a finite element formulation of the convected wave equation. The finite element solution is carried out in cylindrical coordinates for each harmonic of the blade passage frequency. A wave envelope scheme is used to represent the radiation boundary condition both with and without the forward flight effect[12].

If t(r) and m(r) are the thrust and torque components of the propeller blade loading per unit span, given by Eqs. (9) and (10), then the propeller can be replaced by an equivalent volumetric force distribution in the propeller plane given by [8]

$$f_x = \delta(x) \sum_{-\infty}^{\infty} f_{x_\ell} \, e^{i(\eta_\ell t - \ell N\theta)} \tag{18}$$

$$f_{\theta_m} = \delta(x) \sum_{-\infty}^{\infty} f_{\theta_\ell} \, e^{i(\eta_\ell t - \ell N\theta)} \tag{19}$$

where

$$f_{x_\ell} = -(\rho c^2)^{-1}[t(r)/a](N\Omega/2\pi)[\sin(\ell N\Omega t)/\ell N\Omega] \tag{20}$$

$$f_{\theta_\ell} = (\rho c^2)^{-1}[m(r)/a](N\Omega/2\pi)[\sin(\ell N\Omega t)/\ell N\Omega] \tag{21}$$

and $\eta_\ell = \ell N\Omega$. The parameter a is the projection of the blade chord on the propeller disk given by

$$a = c \cos\varphi \tag{22}$$

where c is the local blade chord, φ is the blade twist measuring the angle of the propeller chord plane with respect to the propeller disk plane, and τ is time required for the propeller to sweep by a point on the propeller disk,

$$\tau = a(r)/\Omega r \qquad (23)$$

Equations (18) and (19) show that the volumetric force distribution is periodic with harmonics of the fundamental frequency $N\Omega$. Each temporal harmonic is associated with angular harmonics of the fundamental angular wave length $2\pi/N$. It is important to note that the source harmonic frequencies for the fixed rotational speed Ω are the same as for the structureborne source.

Figure 3 shows a typical propeller noise radiation pattern in the form of contours of constant acoustic pressure magnitude. The contours shown are in a plane of constant θ in a cylindrical coordinate system with the symmetry axis along the propeller axis and with the thrust direction to the right. The contours shown here are for a six-bladed propeller with no forward flight effect. Figure 4 is a cartesian plot of the directivity of the same propeller on a line two propeller radii from the propeller axis. This is the location which is chosen to represent the noise levels to which the cabin sidewall is subjected. The curve of Figure 4 is normalized to 100 dB, but the absolute level is also computed so that the maximum sound pressure level on the reference line is known. This maximum pressure, which can easily be in the range of 105-135 dB, is used as the airborne noise source. In the present study no effort is made to model the actual distribution of sound pressure level on the cabin sidewall and it is assumed that the sound pressure level is constant over the sidewall and is normally incident.

STRUCTURAL MODEL AND COUPLING TO THE CAVITY

The structural model attempts to represent the essential features of the structureborne path of a wing-fuselage system. Both the wing and the fuselage are modelled with finite elements. This is schematically depicted in Figure 5. For simplicity, the fuselage is represented by a rectangular cavity with all sides rigid except for the side adjacent to the wing. The wing is represented by a beam and the fuselage carry-through structure is represented by a heavy vertical stiffener, as shown. The fuselage sidewall is assumed to be clamped at its edges and the model is assumed to be symmetric with respect to the vertical plane formed by the wing and stiffener.

Both the wing and carry-through stiffener are modelled by one-dimensional Hermitian beam elements in bending. Linear extensional properties are also included. Each node has three degrees of freedom: A transverse displacement, a slope, and an inplane axial displacement. The fuselage sidewall is modelled by a series of four-noded sixteen-degree-of-freedom Hermitian flat plate elements [13]. The variables at each node are (w, w_x, w_y, w_{xy}) where w is the transverse displacement and subscripts denote the partial derivative of w with respect to that variable. Figure 6 shows the discretization of the portion of the fuselage panel that was modelled. Symmetry about the vertical stiffener is assumed so that the stiffener is shown at the right boundary of the fuselage panel. In this analysis the fuselage panel is assumed to be stiffened by stringers and frames. However, because these stiffeners are not as large as the structural connection for the wing to the fuselage, they are modelled as smeared stiffeners [14]. In Figure 6, the spacing of the vertical frames and horizontal stringers is d and $\hat{\ell}$, respectively. The finite element model can easily be extended to include discrete frames and stiffeners since the elements used throughout have enough degrees of freedom to enforce all the compatibility conditions. Thus, no growth in dimensionality would be required. In addition, the Bogner, Fox, Schmit [13] elements have been coded to be applicable to cylindrical shell representations for the sidewall. There are obvious possibilities for growth of the present model.

The structural model has been generated with a program written specifically for this problem in order to take full advantage of the coupling techniques introduced. In this section an outline of the procedure is given.

The wing is modelled using Hermitian bending and linear axial deflection. The nodal degrees of freedom are bending deflection, bending slope, and axial deflection. If there are N_w wing elements, then the wing has $3N_w$ degrees of freedom (the degrees of freedom at the attachment point of the wing to the carry-through structure are assigned to the sidewall). These degrees of freedom are designated $\{W_w\}$. The fuselage sidewall (plate) has $4(N_{px}+ 1)(N_{pz}+ 1)$ degrees of freedom, when N_{px} and N_{pz} are the number of elements lengthwise and widthwise, respectively. Each node has four degrees of freedom: w, w_x, w_z, and w_{xz}. The sidewall modal displacement vector is $\{W_p\}$. Note that all of the sidewall degrees of freedom are not active due to the boundary constraint. Note also that stringers, frames, and the carry-through structure will not introduce new degrees of freedom.

The dynamic equations of motion for the wing and sidewall are written as

$$\begin{bmatrix} M_{ww} & M_{wp} \\ M_{pw} & M_{pp} \end{bmatrix} \begin{Bmatrix} \ddot{W}_w \\ \ddot{W}_p \end{Bmatrix} + \begin{bmatrix} K_{ww} & K_{wp} \\ K_{pp} & K_{pp} \end{bmatrix} \begin{Bmatrix} W_w \\ W_p \end{Bmatrix} = \begin{Bmatrix} Q_w \end{Bmatrix} + \begin{Bmatrix} 0 \\ Q_p \end{Bmatrix} \tag{24}$$

The force vector $\{Q_w\}$ is generated from the propeller source model and $\{Q_p\}$ is generated from the cavity acoustic pressure acting on the sidewall. The vector $\{Q_w\}$ cannot be partitioned in terms of wing deflections only, since the wing attachement point degrees of freedom are also assigned to the sidewall. The vector $\{Q_p\}$ is partitioned in terms of the sidewall deflections only. A free vibration analysis, based on Eq. (24), is formulated as

$$\begin{bmatrix} K_{ww} & K_{wp} \\ K_{pw} & K_{pp} \end{bmatrix} \begin{Bmatrix} W_w \\ W_p \end{Bmatrix} = \omega^2 \begin{bmatrix} M_{ww} & M_{wp} \\ M_{pw} & M_{pp} \end{bmatrix} \begin{Bmatrix} W_w \\ W_p \end{Bmatrix} \tag{25}$$

A subspace interation eigenvalue routine was used to solve the eigenvalue problem. This yields a sequence of structural eigenvalues ω_{si}, and a sequence of structural eigenvectors $\{W_s\}_i$, which, when truncated in a suitable way, can be used to generate a modal matrix

$$[\psi] = \left[\{W_s\}_1 \; \{W_s\}_2, \; \ldots \; \{W_s\}_{Ns} \right] = \left\{ \begin{matrix} \psi_w \\ \psi_p \end{matrix} \right\} \tag{26}$$

This modal matrix is partitioned into wing and plate contributions. An eigenvector expansion of Eq. (24) yields

$$\left[\diagdown \, M_{sii} \right] \{\ddot{q}\} + \left[\diagdown \, C_{sii} \right] \{\dot{q}\} + \left[\diagdown \, K_{sii} \right] \{q\} = [\psi_W{}^T \;\vdots\; \psi_p{}^T]\{Q_W\} + [\psi_p]^T\{Q_p\} \tag{27}$$

where

$$\left[\diagdown \, M_{sii} \right] = [\psi]^T \, [M] \, [\psi] \tag{28}$$

is the diagonal generalized mass matrix for the structure and [M] is the original finite element mass matrix. In the calculation of eigenvalues, [M] is normalized so that $M_{sii} = 1$, and $K_{sii} = \omega_i{}^2$. An equivalent viscous modal damping $c_{sii} = 2\zeta_i\omega_i$ is included at this stage. The coupling from the cavity to the plate in the structural equations is through the new generalized force vector

$$\{Q_{sc}\} = [\psi_p]^T\{Q_p\}$$

The form of this vector can be obtained by returning to the definition of $\{Q_p\}$. The virtual work of the cavity pressure on the sidewall is

$$\delta W = \int_{\partial\Omega_s} p(x,z)\,\delta w_p(x,z)\,dS$$

where $p(x,z)$ is the cavity acoustic pressure, $\delta w_p(x,y)$ is the virtual change in the transverse deflection of the plate, and $\partial\Omega_s$ is the sidewall surface area. In terms of the implicit global shape matrix for the finite element representation of the plate

$$\delta w_p(x,z) = [N_p(x,z)]\{\delta \hat{W}_p\}$$

so that

$$\delta W = \{\delta \hat{W}_p\} \int_{\partial\Omega_s} [N_p]^T p(x,z)\,dS$$

The cavity acoustic pressure is given in terms of the cavity modes

$$p(x,z) = [\phi]\{a\}$$

where the modal matrix $[\phi]$ is a suitably truncated sequence of the cavity mode shapes evaluated on the sidewall and $\{a\}$ is a vector of modal amplitude coefficients.

With these observations, the generalized force vector which couples the cavity to the structure is

$$\{Q_{sc}\} = [\psi_p]^T \left(\int_{\partial\Omega_s} [N]^T[\phi]\,dS \right) \{a\} = [D]\{a\}$$

The integration is broken down into subdomains which are the finite elements on the plate surface and the shape function matrix $[N]$ is explicitly defined within these subdomains by the 16 degree-of-freedom plate element shape functions. The coupling matrix is denoted as $[D]$ and has N_s rows and N_c columns, where N_s is the number of retained structural generalized coordinates and N_c is the number of retained cavity modes.

CAVITY MODEL AND COUPLING TO THE PLATE

For the present study the cavity is rectangular in geometry with dimensions a (length), b (height), and c (depth). The cavity is to be represented in terms of analytic acoustic modes calculated for a completely rigid cavity. These modes and the associated natural frequencies can be calculated directly from the three dimensional wave equation. The cavity frequencies are given by

$$\omega_{\ell,m,n} = c_o\pi \left[(\ell/a)^2 + (m/b)^2 + (n/c)^2\right]^{1/2} \qquad (29)$$

where c_o is the speed of sound in the cavity. The frequencies are arranged in a sequence ω_i, $i = 1, 2, \ldots N_c$ in ascending order. The eigenfunctions are

$$\phi_{\ell,m,n}(x,y,z) = \cos(\ell\pi x/a)\cos(m\pi y/b)\cos(n\pi z/c) \qquad (30)$$

where the cavity coordinate system is shown in Figure 5. The eigenfunctions are also ordered in a sequence $\phi_i(x,y,z)$, $i = 1, 2, \ldots N_c$ corresponding to the sequence of eigenvalues. It is important to note that the lowest cavity frequency is $\omega_{0,0,0} = \omega_1 = 0$ and the corresponding cavity mode, or eigenfunction, is $\phi_1(x,y,z) = 1$, that is, uniform pressure.

The cavity modes satisfy the orthogonality condition

$$\int_\Omega \phi_i\phi_j \, d\Omega = M_{cii}\delta_{ij}$$

where

$$\delta_{ij} = \begin{cases} 0 \ , & i \neq j \\ 1 \ , & i = j \end{cases}$$

and

$$M_{cii} = abc \ , \quad \ell = m = n = 0$$

$$M_{cii} = abc/2 \quad , \begin{cases} \ell > 0, \ m = 0, \ n = 0 \\ \ell = 0, \ m > 0, \ n = 0 \\ \ell = 0, \ m = 0, \ n > 0 \end{cases}$$

$$= abc/4 \quad , \begin{cases} \ell > 0, \ m > 0, \ n = 0 \\ \ell = 0, \ m > 0, \ n > 0 \\ \ell > 0, \ m = 0, \ n > 0 \end{cases}$$

$$= abc/8 \quad , \quad \ell > 0, \ m > 0, \ n > 0$$

In this study, M_{cii} is referred to as "acoustic generalized masses" for the cavity, although the units are those of volume.

Coupling of the structure to the cavity is based on a weighted residuals procedure which reduces to the method discussed by Dowell, Gorman, and Smith [9].

The acoustic pressure within the cavity is governed by the wave equation

$$\nabla^2 p = (1/c_o^2) \ p_{tt} \ \text{in} \ \Omega \tag{31}$$

and the boundary condition

$$\nabla p \cdot \vec{n} = -\rho_o w_{tt} \quad \text{on} \ \partial\Omega$$

where Ω is the volume to which Eq. (26) applies, and $\partial\Omega$ is the surface of Ω, with outward normal n, w_{tt} is the outward particle acceleration at the cavity wall, and ρ_o is the density of the air in the cavity. Boundary conditions of relevance include

$$\begin{aligned} \nabla p \cdot \vec{n} &= 0 \quad \text{on } \partial\Omega_H \\ &= -\rho_o w_{tt} \quad \text{on } \partial\Omega_s \\ &= -\rho_o (A/\rho_o c) p_t \quad \text{on } \partial\Omega_\ell \end{aligned} \qquad (32)$$

where $\partial\Omega_H$ represents hard walls, $\partial\Omega_s$ is the flexible sidewall, and $\partial\Omega_L$ represents acoustically lined area where the relation between acoustic pressure and particle velocity is

$$p_t = Z\, w_{tt} \qquad (33)$$

and the nondimensional normal incidence admittance is given by

$$A = \rho_o c_o / Z \qquad (34)$$

where $Z/\rho_o c_o$ is the nondimensional normal incidence impedance.

The solution for acoustic pressure within the cavity is found from a weighted residual statement: Find a function p(x,y,z) from the class of continuous functions which satisfies ($\overline{\nabla p}$ are the values of ∇p on the boundary)

$$\int_\Omega \hat{W}[\nabla^2 p - (1/c_o^2)\, p_{tt}]d\Omega - \int_S \hat{W}[\nabla p - \overline{\nabla p}]\cdot\vec{n}\, dS = 0 \qquad (35)$$

for all test functions $\hat{W}$ from the class of continuous functions, where $\partial\Omega = \partial\Omega_H U \partial\Omega_S U \partial\Omega_L$, w_{tt} takes on the appropriate value on the constituent segments of $\partial\Omega$, and $\nabla\bar{p}$ are the values of ∇p on the boundary, from Eq. (32).

By using the Divergence Theorem twice on the volume integral, and by defining members of the set of test functions W_i to be solutions of the eigenvalue problem

$$\begin{gathered} \nabla^2\phi + (\omega/c)^2\phi = 0 \\ \nabla\phi\cdot\vec{n} = 0 \text{ on } \partial\Omega \end{gathered} \qquad (36)$$

the weighted residuals statement becomes

$$\int_\Omega \phi_i[p_{tt} + \omega_i^2 p]d\Omega = -\rho_o c_o^2 \int_{\partial\Omega_s} \phi_i w_{tt}\, dS - c_o \int_{\partial\Omega_L} \phi_i A\, p_t\, dS \qquad (37)$$

where ϕ_i is an eigensolution to Eq.(36) corresponding to the eigenvalue ω_i. These eigensolutions are defined by Eq.(30).

The function p(x,y,z) is expanded in terms of the complete sequence of functions ϕ_i so that

$$p(x,y,z) = [\phi]\{a\}$$

where $[\phi]$ is a row matrix whose elements are a truncated sequence of the functions ϕ_i defined by Eq. (36) and $\{a\}$ is a column matrix of time-dependent amplitude coefficients.

The acceleration on the sidewall is similarly expanded in terms of the structural eigenfunctions evaluated on the plate surface.

$$w_{tt}(x,z) = [N_p][\psi_p]\{\ddot{q}\}$$

where the row matrix $[N_p]$ is the implicitly-defined shape matrix for the sidewall deflections and $[\psi_p]$ is the sidewall partition of the modal matrix derived from the structural free vibration problem. The vector $\{q\}$ is a vector of time dependent amplitude coefficients for the structural modes. Equation (32) becomes

$$\lceil M_{cii} \rfloor \{\ddot{a}\} + [C]\{\dot{a}\} + \lceil \omega_c{}^2 M_{cii} \rfloor \{a\} = -[D]\{\ddot{q}\} \qquad (38)$$

where

$$\lceil M_{cii} \rfloor = \int_{\Omega} [\phi]^T[\phi]dV$$

$$[C] = c_o \int_{\partial\Omega_L} A[\phi]^T[\phi]\, dS \qquad (39)$$

$$\rho_o c_o{}^2[D] = \rho_o c_o{}^2 \left(\int_{\partial\Omega_s} [\phi]^t[N_p]dS \right) [\psi_p]$$

The diagonal matrix $\lceil M_{cii} \rfloor$ is the "generalized mass matrix" for the cavity (actual units are volume), [C] is generally not diagonal and is the generalized damping matrix (the form here is only valid for harmonic motion since the impedance relation [28] only applies for harmonic motion). The matrix [D] is the coupling matrix and is generally not square. If N_c cavity modes and N_s structural modes are retained in the model, then [D] is $N_c \times N_s$. Note that the matrix [D] which couples the plate into the cavity, appears as $[D]^T$ in the coupling of the cavity into the plate.

THE PROPELLER GENERALIZED FORCE

The conclusion to be drawn from Eq. (17) is that the lift distribution (lift per unit span) induced at a point on the wing can be written in the form

$$\ell_\omega = L \sum_{\ell} f_\ell(\eta) e^{i\ell N\Omega t}$$

where

$$L = (1/2)\rho U^2 c C_{\ell_{\alpha_w}} (\Gamma/2\pi RU)$$

and the nondimensional spanwise distribution functions $f_\ell(y)$ are defined over four regions by Eqs. (1) through (4).

The generalized force is determined by the virtual work integral as in the determination of the acoustic pressure generalized force in Eq.(28). In the case of the propeller loading

$$\delta W = \int_0^S \ell_\omega(x) \ \delta\omega(x) dx$$

where x is the wing spanwise coordinate and S is the span. The wing vertical deflection is given in terms of the implicitly defined global shape matrix $[N_w]$ as

$$w(x) = [N_w]\{W_w\}$$

where $\{W_w\}$ is here defined to include the nodal displacements and bending slope at the attachment point. Then

$$\delta W = \{\delta W_w\}^T \int_o^s [N_w]^T \ell_w(x)dx$$

Consistent with finite element procedures, the integral is carried out over the element subdomains and assembled into the global generalized force so that

$$\delta W = \sum_n \{\delta W_w\}_n \int_n [N_w{}^e]^T \ell_w(x)dx$$

where the integral is over the n^{th} subdomain. The element shape function matrix is $[N_w{}^e]$. The element generalized force vector is thus

$$\{Q_w\}_n = L \sum_\ell \int_n [N_w{}^e]^T f_\ell(\eta)\ e^{i\ell N\Omega t} dx \qquad (40)$$

$$= \sum_\ell \{Q_w\}_{n\ell}\ e^{i\ell N\Omega t} \qquad (41)$$

where

$$\{Q_w\}_{n\ell} = L \int_n [N_w{}^e]^T f_\ell(\eta)dx \qquad (42)$$

It follows that the global generalized force vector is of the form

$$\{Q_w\} = \sum_\ell \{Q_w\}_\ell\ e^{i\ell N\Omega t} \qquad (43)$$

where $\{Q_w\}$ is obtained by assembling the $\{Q_w\}_{n\ell}$ by conventional methods.

THE AIRBORNE GENERALIZED FORCE

The pressure level in the acoustic field of the propeller is given by

$$p(x,r,\theta,t) = \sum_{\ell=-\infty}^{\infty} P_\ell(x,r) e^{i(\ell N\Omega t - \ell N\theta)}$$

The finite element analysis yields the pressure field in each angular harmonic. That is, we obtain $P_\ell(x,r)$ corresponding to the angular harmonic ℓN which is related to the ℓth harmonic of blade passage frequency $\ell N\Omega$.

As shown in Figure 4, the acoustic field of the propeller at a fixed radial distance from the propeller axis shows considerable variation with axial location, that is the propeller radiated field varies for and aft. In the example shown in the figure, the maximum sound pressure level occurs aft of the propeller and is about 13 dB above a second relative maximum which occurs ahead of the propeller.

At the present time little is known about the coupling of the propeller acoustic field and an adjacent structure. The field is neither normally incident nor representable by oblique plane waves in a simple way. In this study we have used the simplest estimate of the driving pressure due to the propeller noise field. The level is taken as uniform on the sidewall at some fraction of the peak level. The results actually reported here use the peak level itself. At lower fractions of the peak level the interior noise results can be expected to be reduced accordingly.

With this assumption the sidewall is subjected to the distributed normal load

$$f(x,z) = -\sum_{\ell} P_\ell \, e^{i\ell N\Omega t}$$

where P_ℓ is the pressure amplitude in the ℓ^{th} harmonic of the blade passage frequency chosen, as noted above. The virtual work expression becomes

$$\delta W = -\{\delta w_p\} \int_{\partial\Omega_s} [N_p]^T \sum_{\ell} P_\ell \, e^{i\ell N\Omega t} dS \qquad (44)$$

At the element level the generalized force is

$$\{Q_s\}_{n\ell} = -\int_n [N_p]^T \, (P_\ell) \, dS \; e^{i\ell N\Omega t} \tag{45}$$

and after assembly the system generalized force is of the form

$$\{Q_s\} = \sum_\ell \{Q_s\}_\ell \, e^{i\ell N\Omega t} \tag{46}$$

which is again a superposition of harmonics of the blade passage frequency.

THE COUPLED EQUATIONS OF MOTION

The system equations of motion can now be written. For the structural system

$$\left\lceil M_{sii} \right\rfloor \{\ddot{q}\} + \left\lceil 2\zeta_i \omega_{si} M_{sii} \right\rfloor \{\dot{q}\} + \left\lceil \omega_{si}{}^2 M_{sii} \right\rfloor \{q\} - [D]^T\{a\} = \{Q_I\} \tag{47}$$

For the acoustic cavity

$$\left\lceil M_{cii} \right\rfloor \{\ddot{a}\} + [c]\{\dot{a}\} + \left\lceil \omega_{ci}{}^2 M_{cii} \right\rfloor \{a\} + \rho_o c_o{}^2 [D]\{\ddot{q}\} = \{0\} \tag{48}$$

The structural system consists of N_s equations and the cavity system consists of N_c equations. Equations (47) and (48) thus represented a system of $(N_s + N_c)$ equations set up for dynamic response calculated with the input vector

$$\{Q_I\} = [\psi]^T\{Q_w\}$$

or (49)

$$\{Q_I\} = [\psi]^T\{Q_s\}$$

Reference to equations (43) and (46) show that $\{Q_I\}$ can be written in terms of its frequency components

$$\{Q_I\} = \sum_\ell \{Q_I\}_\ell \, e^{i\ell N\Omega t} \tag{50}$$

where for structureborne inputs

$$\{Q_I\}_\ell = [\psi]^T\{Q_w\}_\ell$$

and for airborne inputs

$$\{Q_I\}_\ell = [\psi]^T\{Q_s\}_\ell$$

COMPUTATIONAL RESULTS

In this report, results are presented for the comparison of interior levels for structureborne and airborne noise for several cases of the structural stiffness and mass parameters. For this purpose we have chosen a specific propeller model with the following characteristics:

Number of blades - 4
Radius - 7 ft. (2.133 m)
Blade chord (constant) - 1 ft. (.305 m)
Blade section lift coefficient - 2π
Thrust - 4000 lb (17800 N)
RPM Range - 750-1500 RPM
Tip-Fuselage clearance - 7 ft. (2.133 m)
Flight Mach number - 0.27
Speed of sound - 1125 ft/sec. (343 m/sec.)

The thrust is held constant for the range of propeller speeds so that the blade twist and loading varies with RPM for this study. This also means that the top loading and therefore the trailing vortex strength varies with RPM.

The wing model employed is one of span 29.5 ft (9 m) and chord 7 ft. (2.133 m) with a section lift coefficient of 2π. The propeller axis is located 18 ft. (5.5 m) from the wing root. The reference point for specification of the airborne noise level is at 14 ft. (4.27 m) from the propeller axis. This is a somewhat arbitrary choice in that it places the effective wing root inside the fuselage sidewall, however, only minor changes in interior levels due to the airborne noise are associated with this choice.

Figure 7 shows the computed maximum sound pressure levels in the radiated field of the propeller at two propeller radii from the axis. Levels are shown for the first three harmonics over a propeller speed range of 750 - 1500 RPM. For the propeller chosen, the maximum speed is close to sonic tip velocity. Particularly at the lower rotational speeds the sound pressure level drops off rapidly with increasing harmonic number. The levels shown in Figure 7 are used as the input for the computation of the airborne contribution to interior noise.

The interior cavity is 19.7 ft (6 m) in length, 6.88 ft (2.1 m) in height, and 7.87 ft (2.4 m) in depth. The acoustic characteristics of the cavity are such that 80 acoustic modes cover the frequency range up to 320 Hz.

The structural properties of importance are the mass and stiffness of the wing and carry through structure, and the mass and stiffness properties of the sidewall. All results presented here are for one sidewall configuration. The sidewall is taken as an aluminum plate of thickness approximately .080 in. (.002 m). Relatively light frames and stringers are treated as smeared mass and stiffness yielding a stiffness properties matrix

$$[D] = \begin{bmatrix} D_x & D_{xy} & 0 \\ D_{xy} & D_y & 0 \\ 0 & 0 & D \end{bmatrix} \qquad (51)$$

where

$$D_x = D + (E_s I_s/d) = Eh^3/[12(1-\upsilon^2)] + (E_s I_s/d) = 16.4\text{x}10^3 \text{ lb-ft } (22.3\text{x}10^3 \text{ N-m})$$

$$D_y = D + (E_f I_f/\hat{\ell}) = 10.2\text{x}10^3 \text{ ft-lb } (13.9\text{x}10^3 \text{ N-m})$$

$$D_{xy} = \upsilon D = 12.9 \text{ ft-lb } (17.5 \text{ N-m})$$

$$[(1-\nu)/2]\ D = 13.1 \text{ ft-lb } (17.8 \text{ N-m})$$

The smeared mass of the plate is

$$M_e = M_p + (\rho_s I_s/d) + (\rho_f A_f/\hat{\ell}) = 0.054 \text{ slugs/ft}^2\ (8.55 \text{ kg/m}^2)$$

In Eqs. (51) and (52), E_s and E_f are the Young's modulus for the stiffeners and frames, I_s and I_f are the cross-sectional area moments of inertia of the stiffeners and frames, d and $\hat{\ell}$ are the element edge lengths corresponding to the stiffeners and frames, ρ_s and ρ_f are the mass per unit length of the stiffeners and frames, A_s and A_f are the cross-sectional areas of the stiffeners and frames, and M_p is the plate mass per unit area. The plate Young's modulus is E and the plate thickness is h. Eight cases of wing and carry-through structure stiffness and mass have been considered:

<u>Case I</u>: Stiff Light Wing and Light Carry Through

Wing: $EI = 10^9$ lb-ft^2 (0.414×10^9 N-m^2)

$\rho = 1.13$ slugs/ft (54 kg/m)

Carry Through: $EI = 10^9$ lb-ft^2 (0.414×10^9 N-m^2)

$\rho = 1.13$ slugs/ft (54 kg/m)

Wing Fundamental Frequency = 19 Hz

<u>Case II</u>: Flexible, Heavy Wing and Stiff, Light Carry Through

Wing: $EI = 0.5 \times 10^9$ lb-ft^2 (0.207×10^9 N-m^2)

$\rho = 5.63$ slugs/ft (270 kg/m)

Carry Through: $EI = 10^9$ lb-ft^2 (0.414×10^9 N-m^2)

$\rho = 1.13$ slugs/ft (54 kg/m)

Wing Fundamental Frequency = 6 Hz.

Case III: Flexible, Heavy Wing and Flexible, Heavy Carry Through

Wing: EI = 0.5×10^6 lb-ft^2 (0.207×10^6 N-m^2)

ρ = 5.63 slugs/ft (270 kg/m)

Carry Through: EI = 0.5×10^6 lb-ft^2 (0.207×10^6 N-m^2)

ρ = 5.63 slugs/ft (270) kg/m)

Wing Fundamental Frequency = 0.2 Hz.

Case IV: Flexible, Heavy Wing and Flexible, Light Carry Through

Wing: EI = 0.5×10^6 lb-ft^2 (0.207×10^6 N-m^2)

ρ = 5.63 slugs/ft (270 kg/m)

Carry Through: EI = 10^6 lb-ft^2 (0.414×10^6 N-m^2)

ρ = 1.13 slugs/ft (54 kg/m)

Wing Fundamental Frequency = 0.2 Hz.

Case V: Case I with Acoustic Damping

A = 0.5, where A is defined by equation (34).

Case VI: Realistic Wing and Realistic Carry Through

Wing: EI = 10^8 lb-ft^2 (0.413×10^8 N-m^2)

ρ = 4.532 slugs/ft (217 kg/m)

Carry Through: EI = 10^8 lb-ft^2 (0.413×10^8 N-m^2)

ρ = 4.532 slugs/ft (217 kg/m)

Wing Fundamental Frequency = 3 Hz.

Case VII: Realistic Wing and More Flexible Carry Through

Wing: EI = 10^8 lb-ft^2 (0.413×10^8 N-m^2)

ρ = 4.532 slugs/ft (217 kg/m)

Carry Through: EI = 0.5×10^8 lb-ft (0.206×10^8 N-m)

ρ = 4.532 slugs/ft (217 kg/m)

Wing Fundamental Frequency = 3 Hz.

Case VIII: Realistic Wing and Stiffer Carry Through

Wing: EI = 10^8 lb-ft^2 (0.413×10^8 N-m^2)

ρ = 4.532 slugs/ft (217 kg/m)

Carry Through: EI = 2×10^8 lb-ft (0.826×10^8 N-m)

ρ = 4.532 slugs/ft (217 kg/m)

Wing Fundamental Frequency = 3 Hz.

Case I represents a very stiff and relatively light wing and carry-through structure. Case II is a somewhat less stiff, but significantly more massive wing structure with the carry-through structure of Case I. Cases III and IV are at the other extreme. Both have a flexible, relatively massive wing structure. In Case III the carry-through structure is flexible and massive while in Case IV it is flexible and relatively light. While not conforming to any existing structures, these cases should at least bound realistic configurations. Case V is just Case I with interior acoustic damping. Cases VI, VII and VIII are much closer to realistic structures. Case VI establishes a representative wing and carry-through system. In Case VII, the stiffness of the carry-through structure is one-half of that of Case VI; in Case VIII, it is twice as stiff as in Case VI.

The structural model for the dynamic response calculations is based on a subset of the structural eigenvalues and eigenvectors spanning a frequency range in excess of 1000 Hz. In the present study we have not included structural damping and we have not included dissipation within the cavity. Structural damping has the primary effect of limiting the resonant response. It is not quantifiable with any degree of certainty.

Any effort to assess the interior noise levels on the basis of resonant response amplitude is not appropriate due to the sensitivity of the response amplitude to damping. Our assessment of the relative levels of interior noise from the airborne and structureborne sources is based on a comparison of the non-resonant response, that is, a comparison of the general levels of the response.

For both structureborne and airborne inputs, equation (50) shows that the generalized force is a superposition of harmonics of the fundamental frequency $N\Omega$. In the present study we retain three harmonics since it has been found that the nonresonant response levels are reasonably well defined with this limited representation of the input. The interior response will also exhibit the harmonics of the fundamental. The overall acoustic pressure level can therefore be represented simply in terms of the amplitudes of the harmonics according to

$$p^2 = \frac{1}{T}\int_o^T |p|^2 \, dt = \left\{ \sum_{i=1}^{3} |p_i|^2 \right\}^{1/2} \tag{53}$$

where p_i is the amplitude of the pressure response at the measurement point for the i^{th} harmonic of the fundamental frequency $N\Omega$ and p^2 is the average square amplitude of the response pressure.

The results of calculations for Cases I through VIII are shown in Figures 8-25. These figures show the interior noise level at a point adjacent to the fuselage side wall in the center of the sidewall. The response is shown as a function of propeller rotational speed in RPM. At each RPM the input has many harmonics (three have been considered here) so that the noise level is defined by equation (53) superimposing the effects of the harmonics. On Figures 8-11, the structureborne and airborne levels are shown separately. Note that the two curves have some resonant peaks in common and others at different frequencies. This is because of the different nature of the structureborne and airborne generalized forces and the modes (both cavity and structural) which they excite. Shown superimposed on the response curves are interpretations of what we define as the general level of the nonresonant response which because of the uncertainty in structural damping level is used to assess the comparison between the two noise sources.

Figure 8 shows the results for Case I in which the wing and carry-through structure is very stiff. The wing cantilevered fundamental frequency is 19 Hz. It is noted in this case that the structureborne noise creates levels substantially below those related to airborne noise.

In Case II, shown on Figure 9, the wing is considerably less stiff than in Case I. The cantilevered fundamental frequency is 6 Hz. The carry-through structure is still extremely stiff and light. The interior levels in this case are still dominated by the airborne noise.

In the third and fourth cases, the wing and carry-through structure are very flexible. The cantilevered wing fundamental frequency is 0.2 Hz in both cases, perhaps a factor of ten below actual wing characteristics. In Case III the carry-through structure is less stiff than in Case IV. Figures 10 and 11 show that the interior noise level contributions of the structureborne and airborne sources become much more similar, particularly at the lower propeller speeds where the two levels are about the same.

It is clear that the stiffness and mass of the wing and carry-through structure are of central importance in the transmission of structureborne noise into the fuselage. In all four cases the airborne noise level is relatively unaffected by the wing and carry-through structural characteristics. However, the structureborne noise level is strongly dependent on these characteristics. The structureborne levels generally decrease with an increase in the stiffness of the wing and carry-through structure.

Figures 12 and 13 show the effect of interior acoustic damping on airborne and structureborne noise. In both cases, damping (as expected) is seen to damp out peaks. Especially affected are those peaks that are due to acoustic resonances.

Figures 14-16 are for the more realistic wing and carry-through structure. For these cases, airborne noise is significantly higher than structureborne noise. These results are consistent with the previous cases in the sense that lower structureborne noise levels are associated with increased stiffnesses of the carry-through structure.

Figures 17-19 show airborne noise levels when the fuselage is only partially loaded. In these calculations, the cases VI, VII, and VIII are repeated with only the panel loaded in a centrally-located vertical strip covering 60% of panel area. Both damped and undamped cases have been computed. Comparison with Figures 14-16 indicates that there is only an insignificant change in the airborne noise levels when the panel is only partially loaded.

In Figures 20-25, the effect of various damping levels is shown on the airborne and structureborne noise levels for cases VI-VIII. As expected, the damping reduces peaks in the response that result from cavity and structure resonances. The meaning of A is given by equation (34).

CONCLUSIONS

A simple, though physically meaningful, model for assessing the relative importance of structureborne and airborne contributions in interior noise levels for propeller driven aircraft has been created. The system for which dynamic response calculations are made consists of a cavity model, a structural model, a model for the propeller radiated acoustic field, and a model for the propeller trailing vortex mechanism which excites the structureborne noise. The dynamic response model is based on the cavity modes and frequencies and the wing - carry through structure - sidewall modes and frequencies with suitable coupling. The forcing function is synthesized from the generalized forces associated with the propeller radiated field and the trailing vortex system.

Computational results indicate that the relative importance of the two source mechanisms depend strongly on the stiffness and mass properties of the wing carry-through structure. For stiff structures the structureborne interior noise levels are well below the airborne levels. For very flexible structures the interior levels from the two source mechanisms can be comparable.

Both the geometry of the structural model and the stiffness and mass properties have been changed for the purpose of investigating different configurations with the goal of more effectively bracketing the characteristics encountered in actual aircraft installations. The structural model can employ structural damping or equivalent viscous damping. At this stage we have chosen not to use it because of lack of quantifiable data. The cavity model did include dissipation due to acoustic treatment. The effect of internal absorption was studied.

The noise source models are constructed so that simple data changes allow for the variation of all important propeller parameters. It is a simple matter to investigate propellers of any radius and any number of blades, positioned as required relative to the fuselage.

ACKNOWLEDGEMENT

The research program reported here has been supported under research grant NASA NAG 1-394 from Langley Research Center.

REFERENCES

1. L. R. Koval 1980 Journal of Sound and Vibration 71, 511-521. On sound transmission into a stiffened cylindrical shell with rings and stringers treated as discrete elements.
2. J. S. Mixson and C. A. Powell 1984 AIAA Paper 84-2349. Review of recent research on Interior Noise of Propeller Aircraft.
3. J. F. Wilby 1983 SAE Paper 830737. The prediction of interior noise of propeller driven aircraft: a review.
4. V. L. Metcalf and W. H. Mayes 1983 SAE Paper 830735. Structureborne contributions to interior noise of propeller aircraft.
5. J. F. Unruh 1979 NASA CR 159099. Engine induced structureborne noise in a general aviation aircraft.
6. M. C. Junger, J. M. Garrelick, R. Martinez, and J. E. Cole, III 1984 NASA Contractor Report 172391. Analytical model of the structureborne interior noise induced by a propeller wake.
7. M. C. Junger and D. Feit 1971 Sound, Structures, and Their Interaction, MIT Press, Cambridge, Mass.
8. W. Eversman and J. E. Steck 1984 AIAA Paper 84-2286. Finite element modelling of acoustic singularities with application to near and far field propeller noise.
9. E. H. Dowell, G. F. Gorman, III and D. A. Smith 1977 Journal of Sound and Vibration 52(4), 519-542. Acoustoelasticity: General theory, acoustic natural modes and forced response to sinuosity excitation, including comparisons with experiment.
10. K. E. Heitman and J. S. Mixson 1986 AIAA Paper 86-0390. Laboratory study of the effects of sidewall and source directivity on the interior noise of a light aircraft fuselage.

11. D. O. Dommasch, S. S. Sherby, and T. F. Connolly 1967 Airplane Aerodynamics, Fourth Edition, Pitman Publishing Corporation, New York, 211-243.

12. A. V. Parrett and W. Eversman 1984 AIAA Paper 84-2333. Applications of finite element and wave envelope element approximation to turbofan engine noise radiation including flight effects.

13. F. K. Bogner, L. R. Fox, and L. A. Schmit 1966 Proceedings of the Conference on Matrix Methods in Structural Mechanics, AFFDL-TR-66-80. The generation of inter-element compatible stiffness and mass matrices by the use of interpolation formulas.

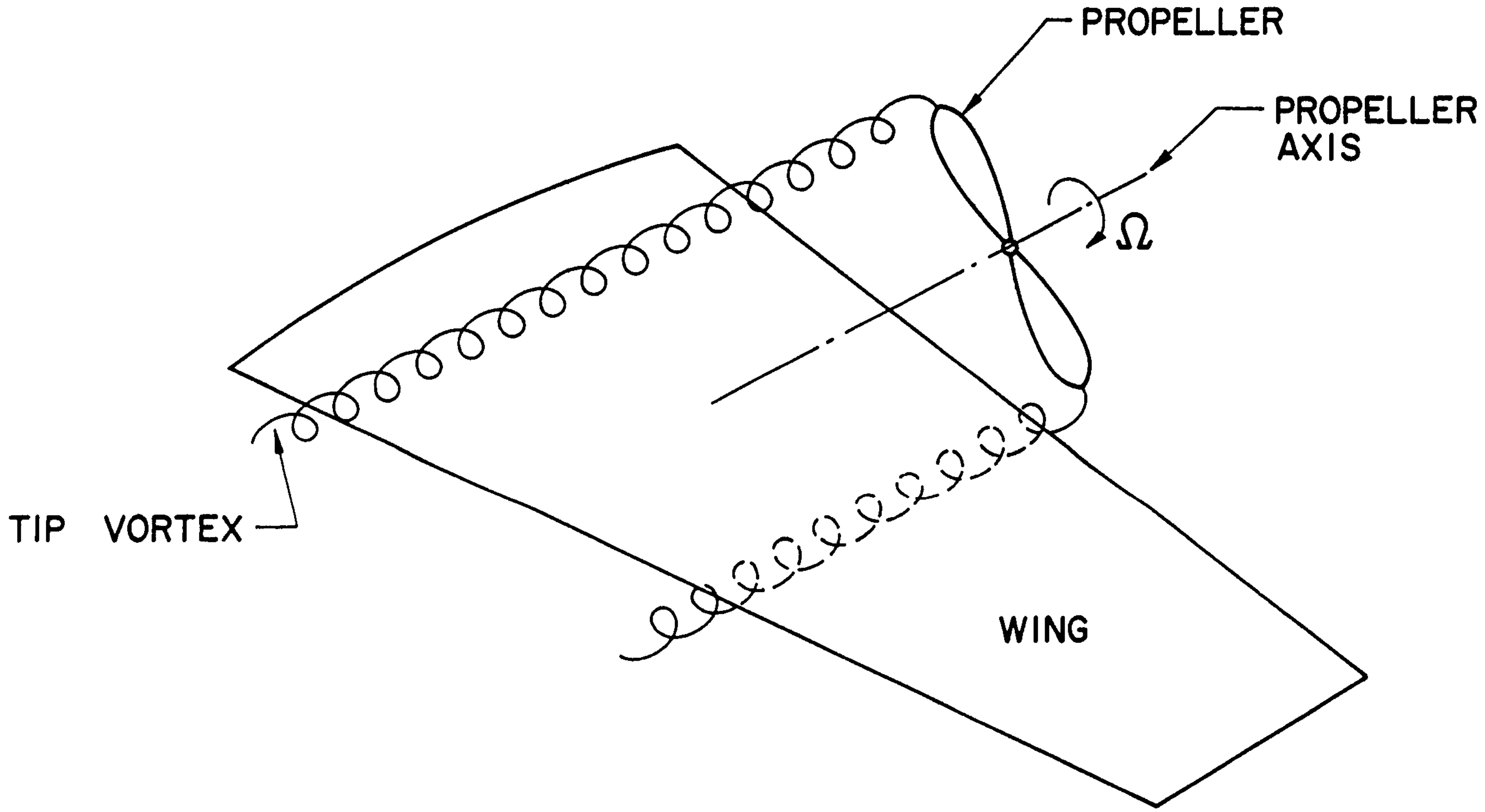

Figure 1. The Vortex Model for the Propeller Structureborne Noise Source

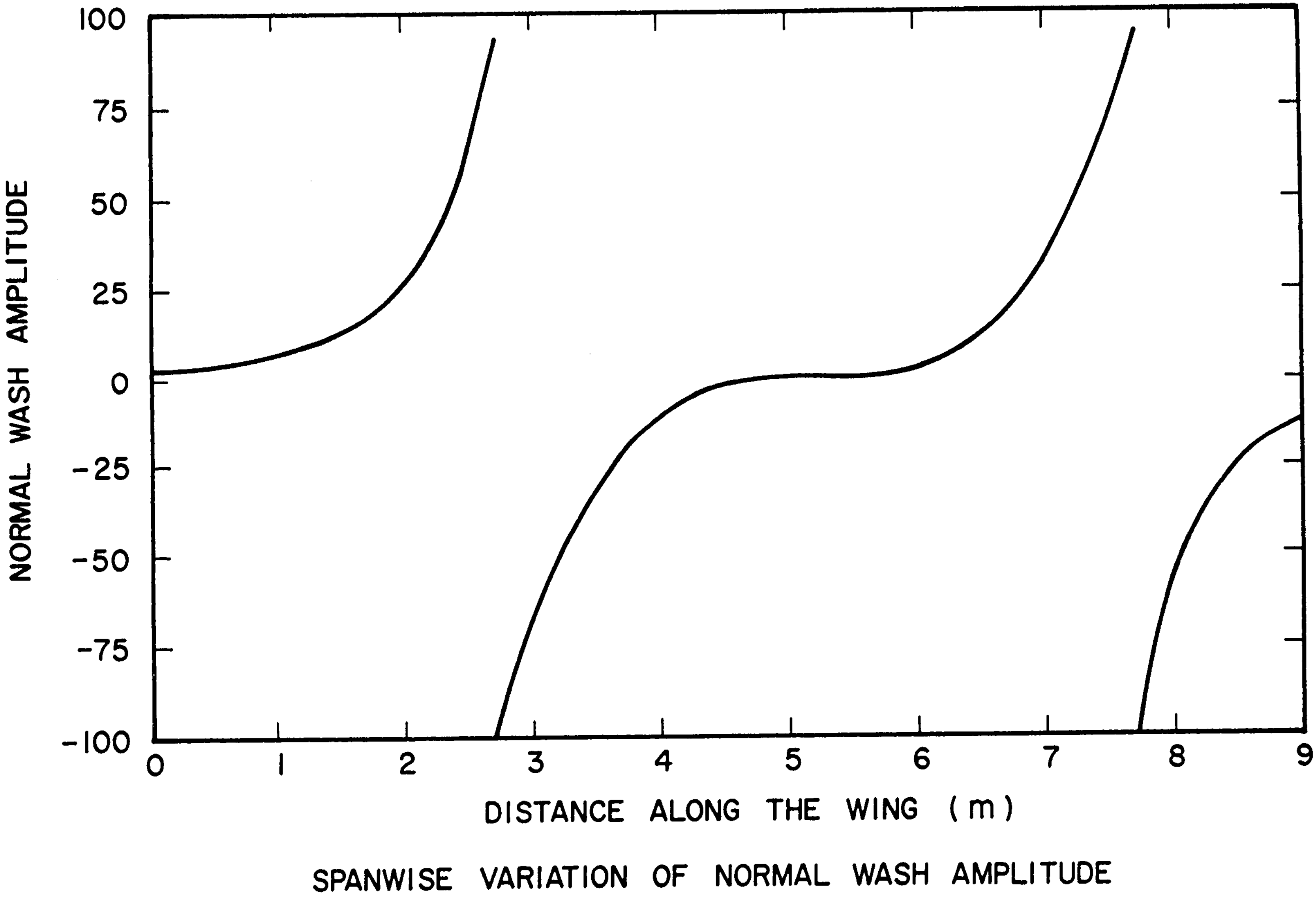

Figure 2. A typical variation of normalwash amplitude in the first harmonic on the wing surface due to the trailing vortex system. Propeller diameter is 2.5 m with axis at 5 m from the wing root.

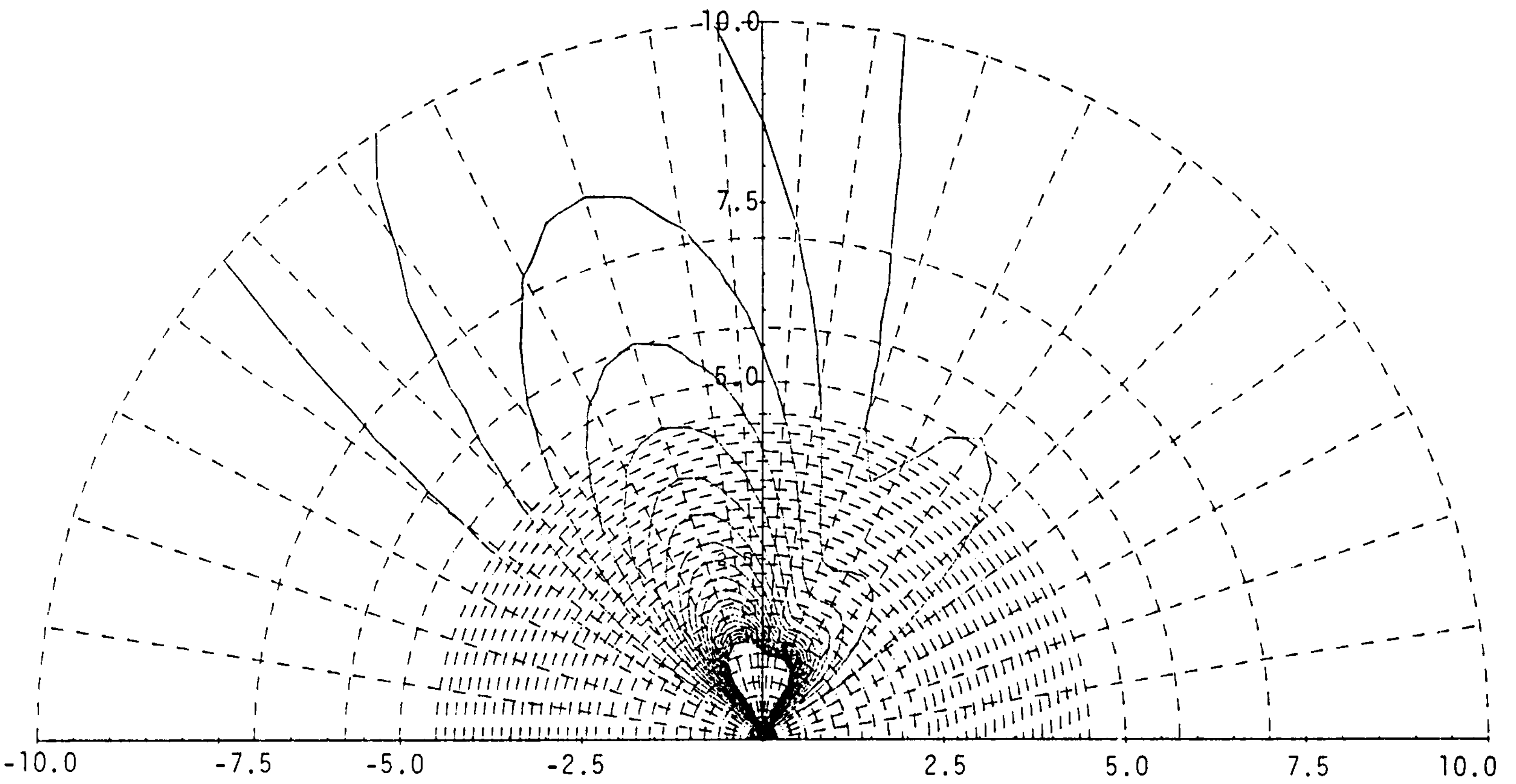

Figure 3. A typical propeller radiation pattern. Contours of constant acoustic pressure magnitude. The propeller has six blades and the tip speed is approximately sonic.

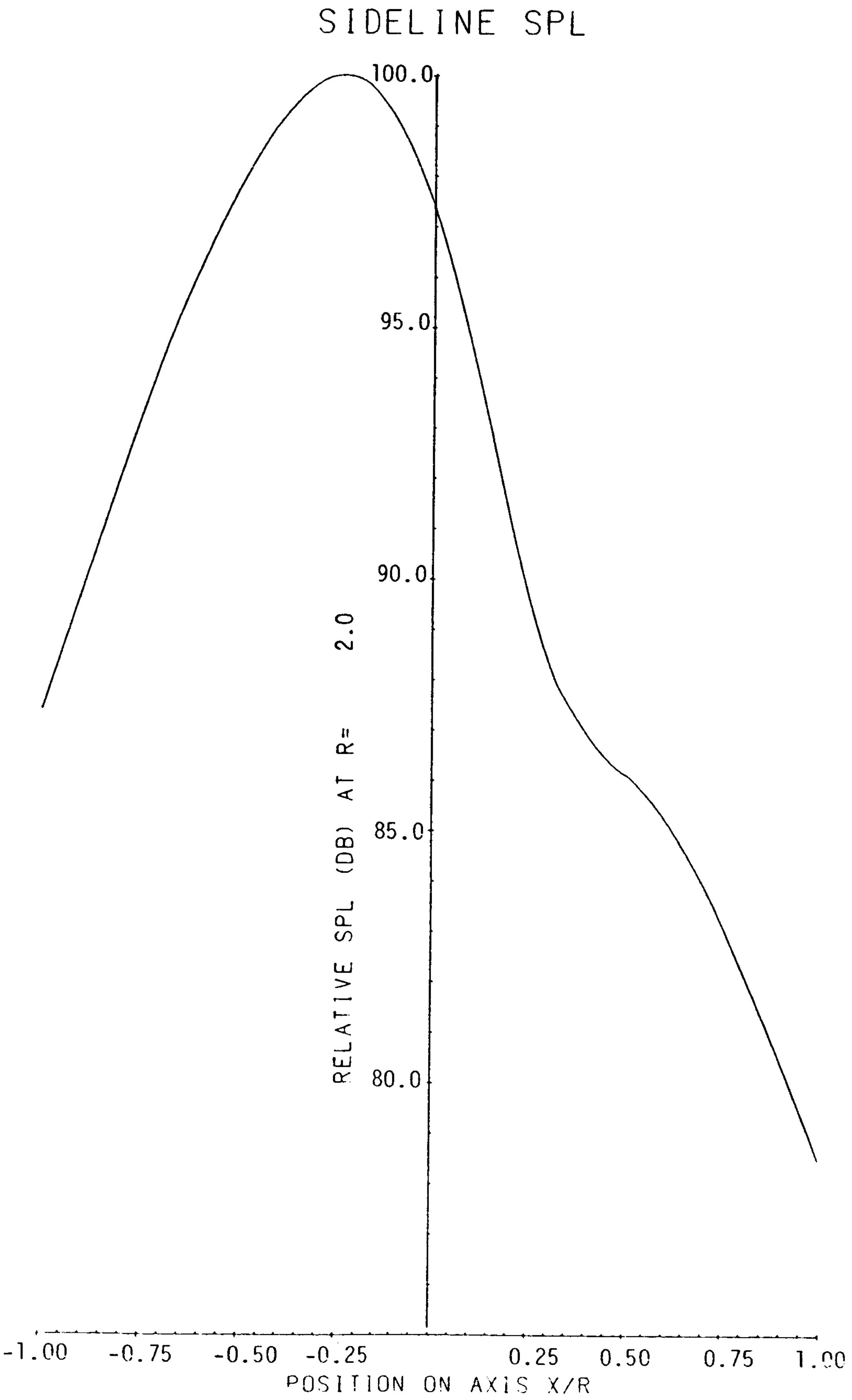

Figure 4. Sideline propeller directivity at two propeller radii from the axis.

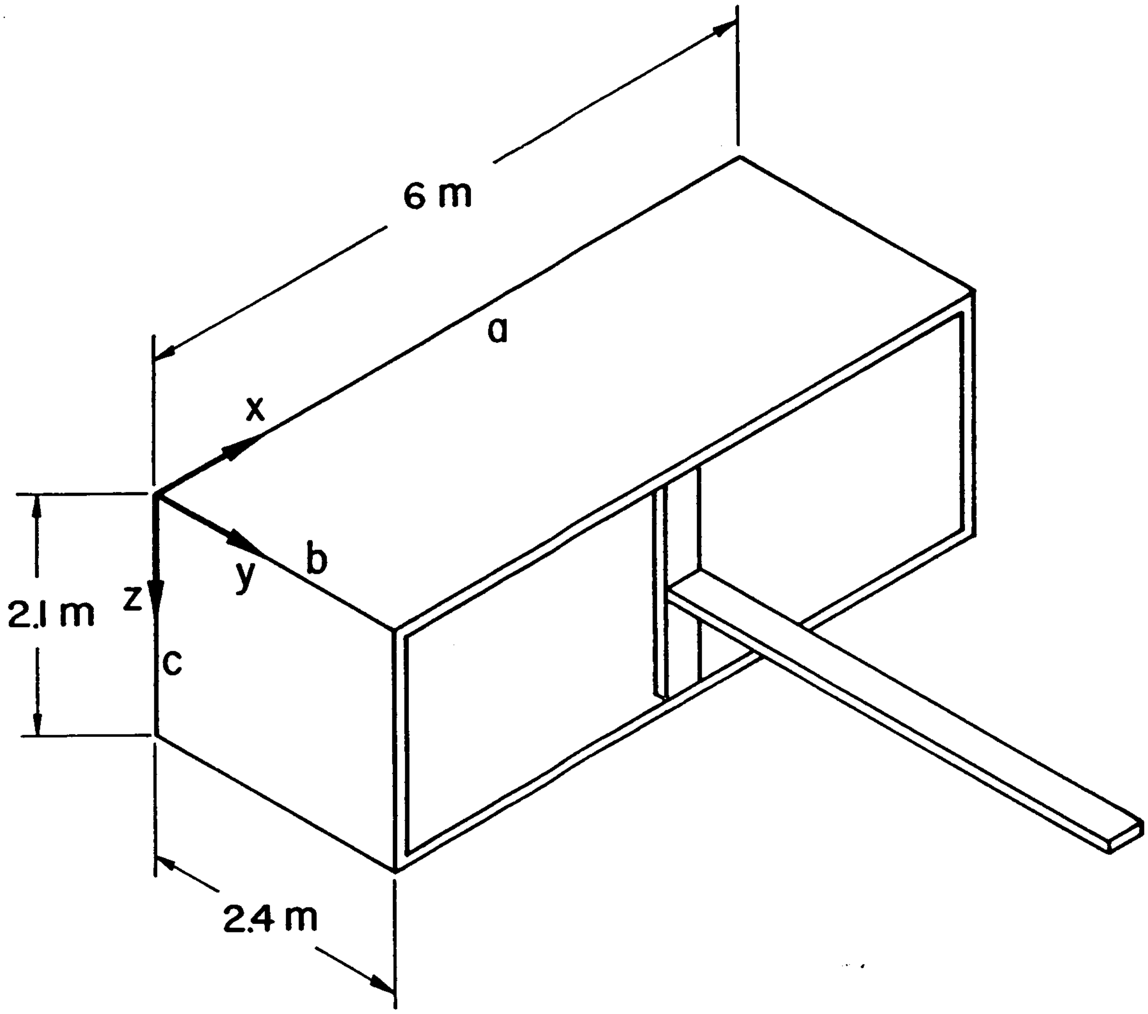

Figure 5. The idealized structural model with the fuselage cavity modelled by a rectangular cavity with a flexible side wall. The wing is modelled as a beam carried into the fuselage by a discrete sitffener.

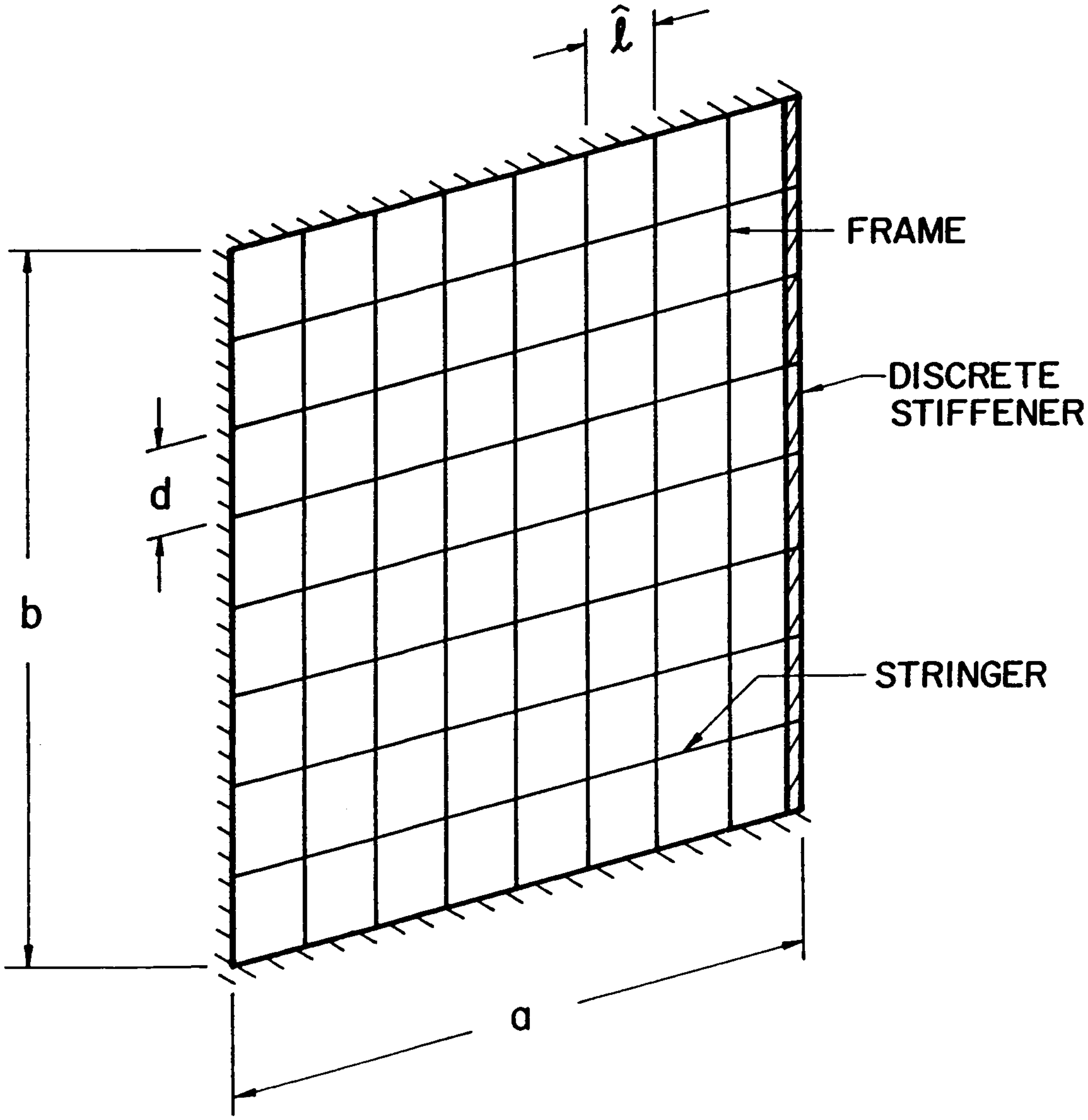

Figure 6. The finite element model of the fuselage side wall showing the element subdivisions and the discrete stiffener for the carry-through structure. The elements can have smeared or discrete stiffeners.

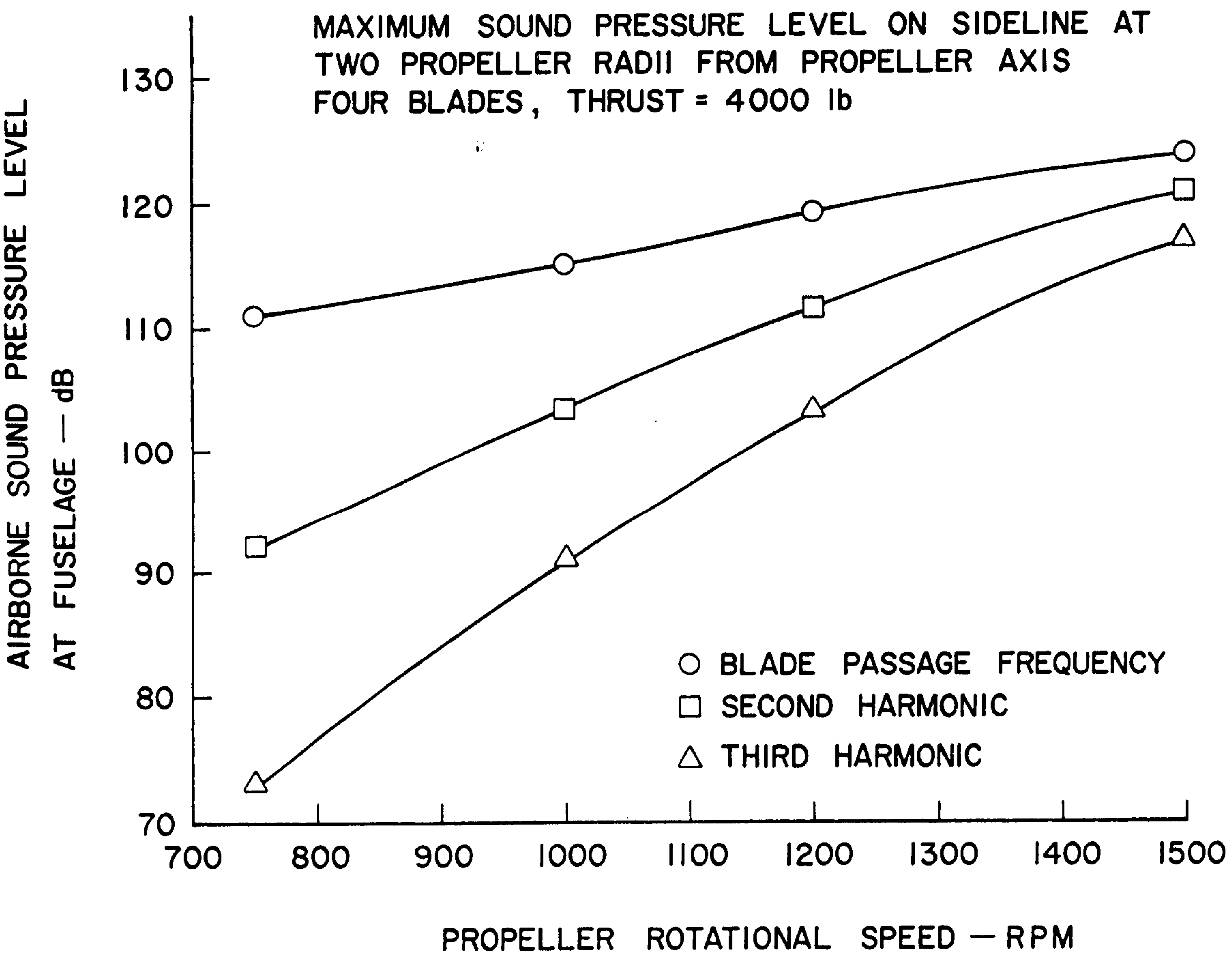

Figure 7. The airborne noise source strength in the first three harmonics as a function of RPM for fixed thrust.

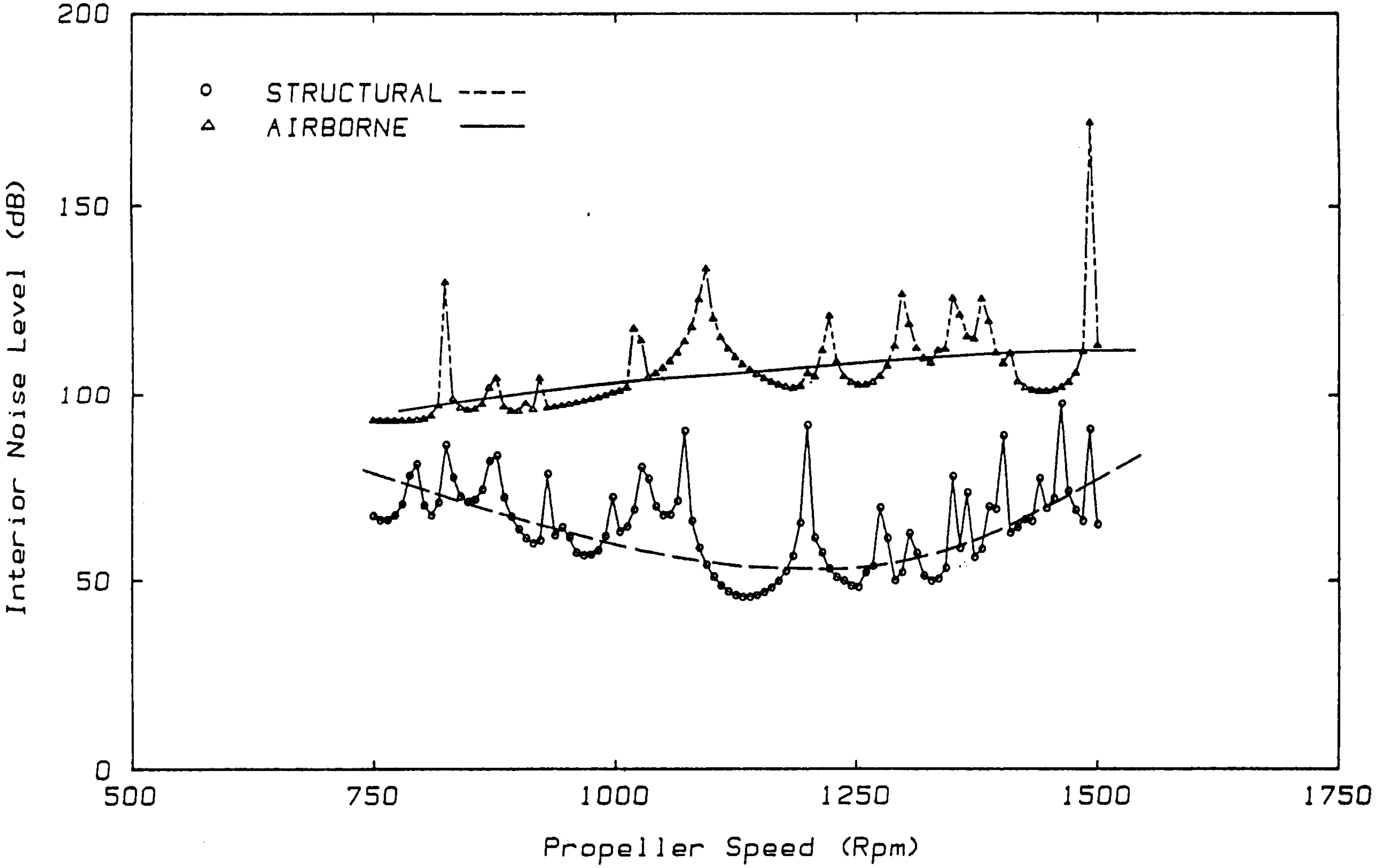

STRUCTURAL AND AIRBORNE NOISE TRANSMISSION (CASE I)

Figure 8. Interior noise levels for structural model, Case I, as a function of propeller RPM at constant thrust.

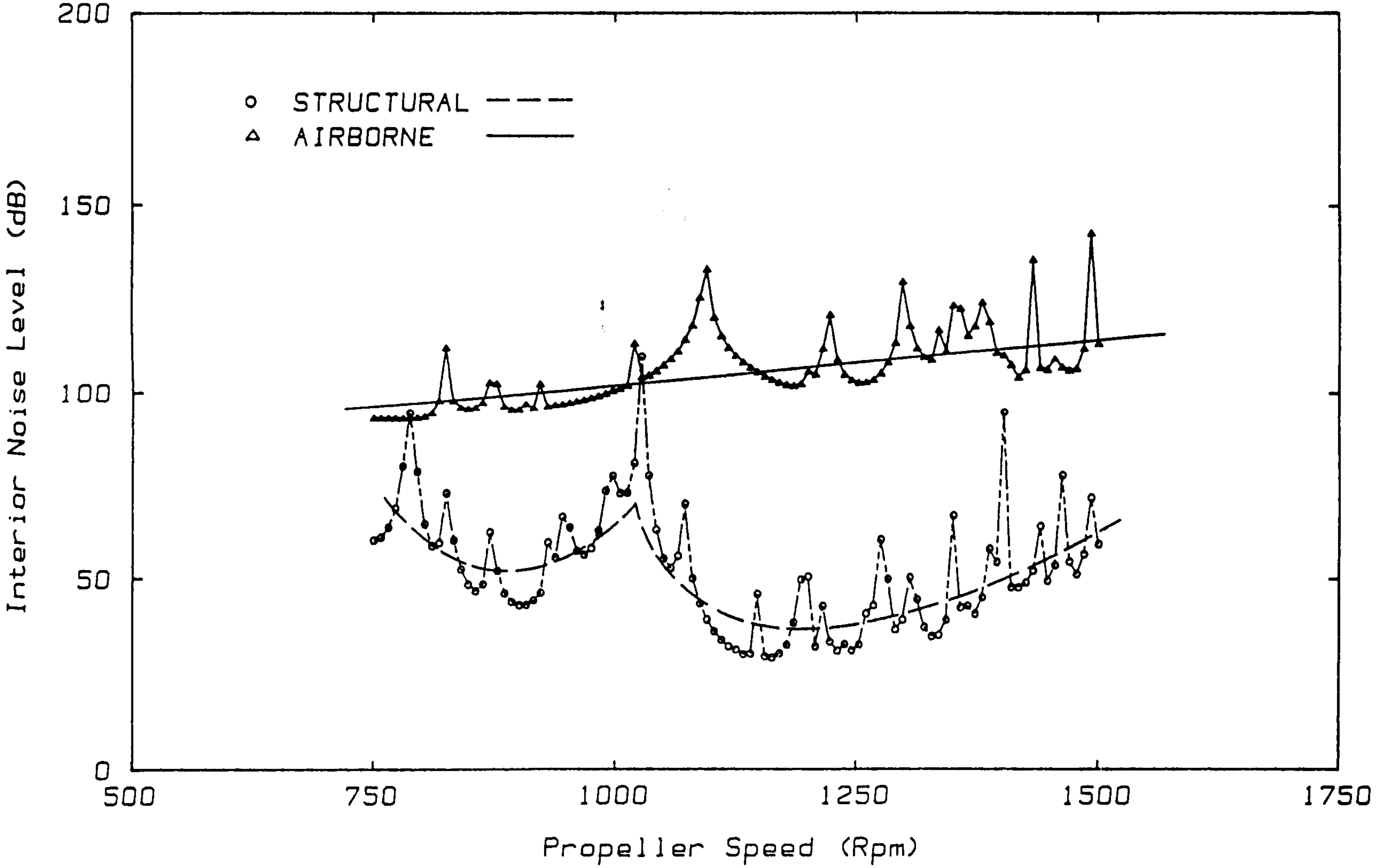

STRUCTURAL AND AIRBORNE NOISE TRANSMISSION (CASE II)

Figure 9. Interior noise levels for structural model, Case II, as a function of propeller RPM at constant thrust.

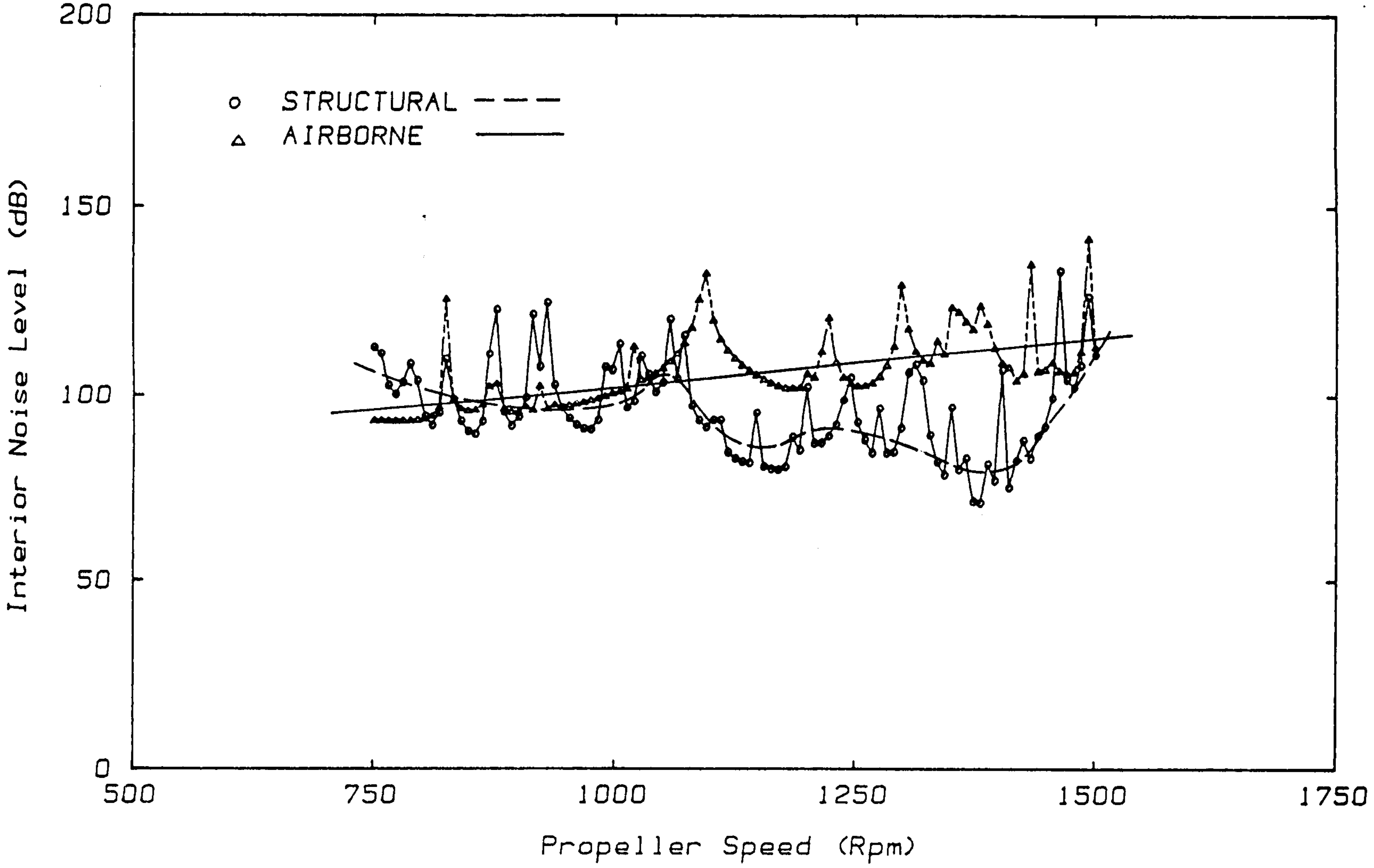

STRUCTURAL AND AIRBORNE NOISE TRANSMISSION (CASE III)

Figure 10. Interior noise levels for structural model, Case III, as a function of propeller RPM at constant thrust.

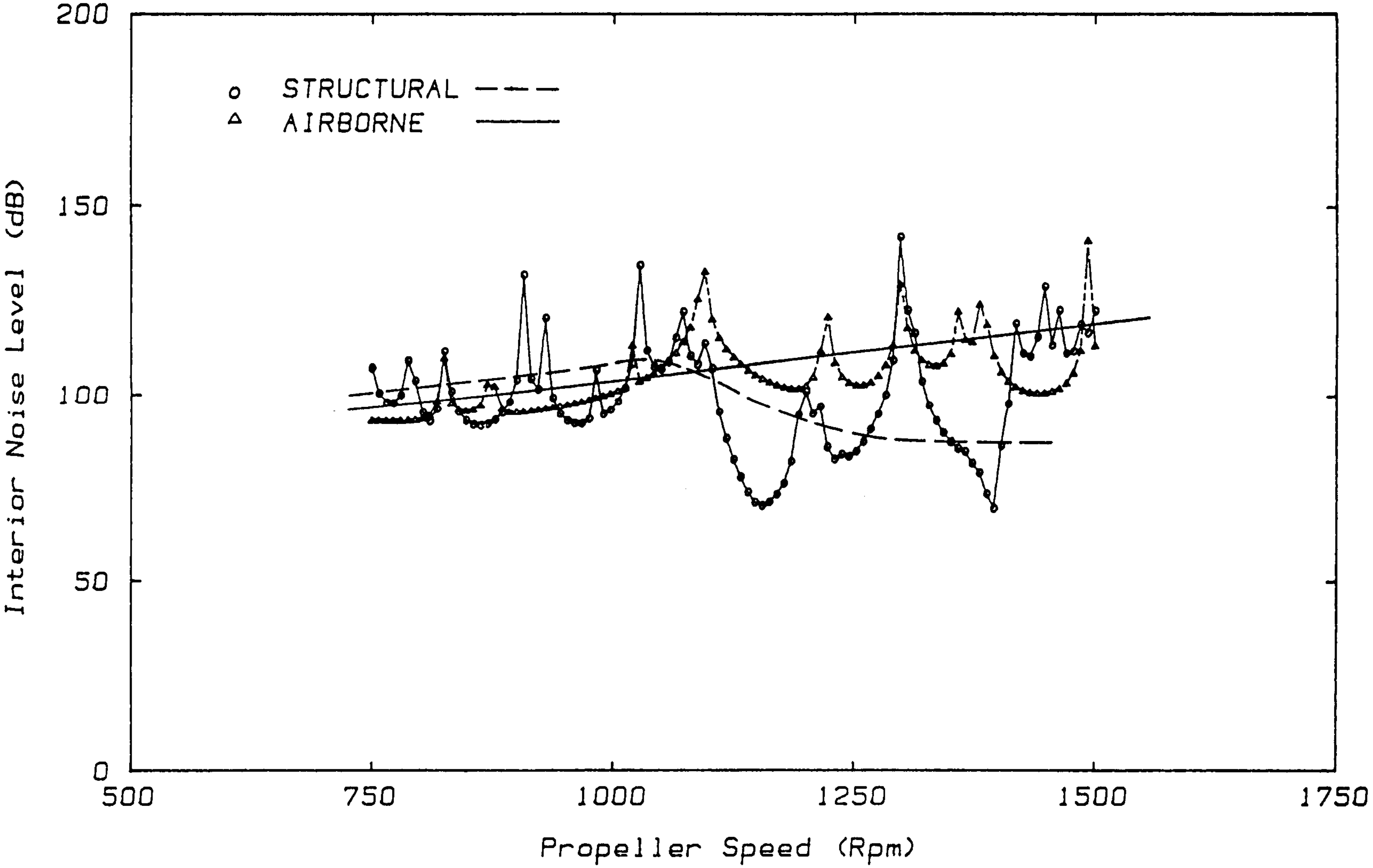

STRUCTURAL AND AIRBORNE NOISE TRANSMISSION (CASE IV)

Figure 11. Interior noise levels for structural model, Case IV, as a function of propeller RPM at constant thrust.

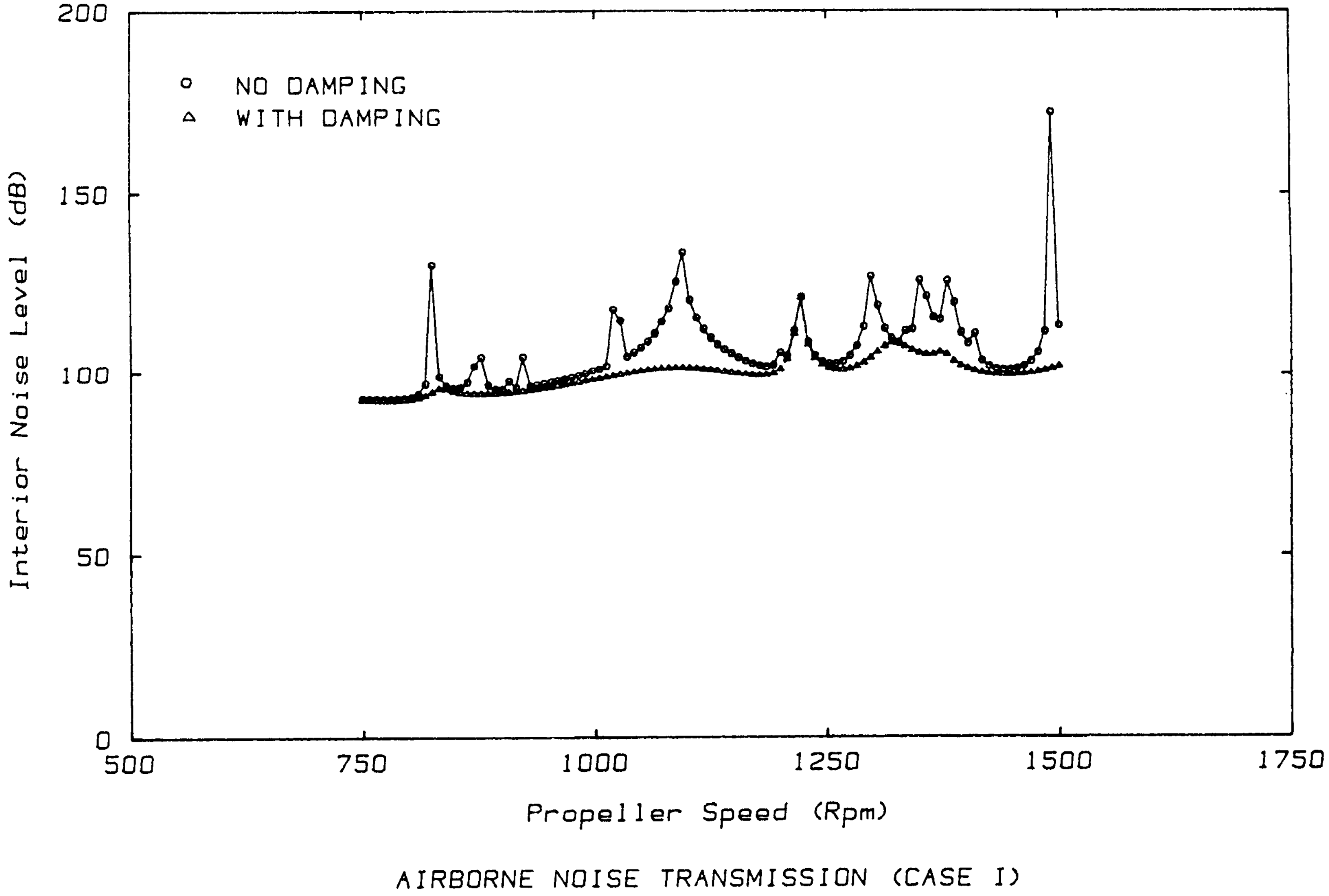

Figure 12, Effect of intrior absorption on interior noise levels due to airborne noise transmission for the structural model of Case I.

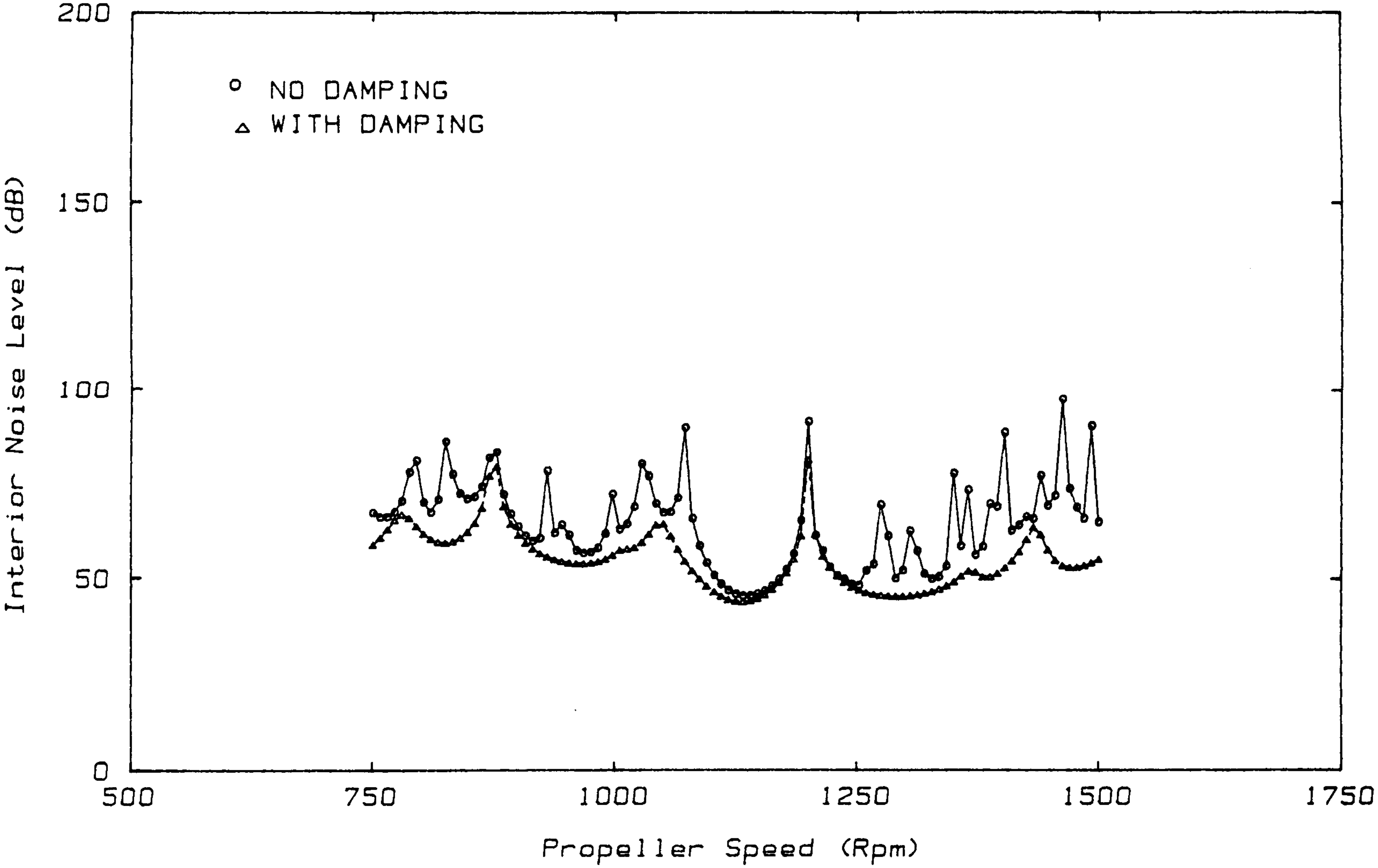

STRUCTURAL NOISE TRANSMISSION (CASE I)

Figure 13. Effect of interior absorption on interior noise levels due to structurborne noise transmission for the structural model of Case I.

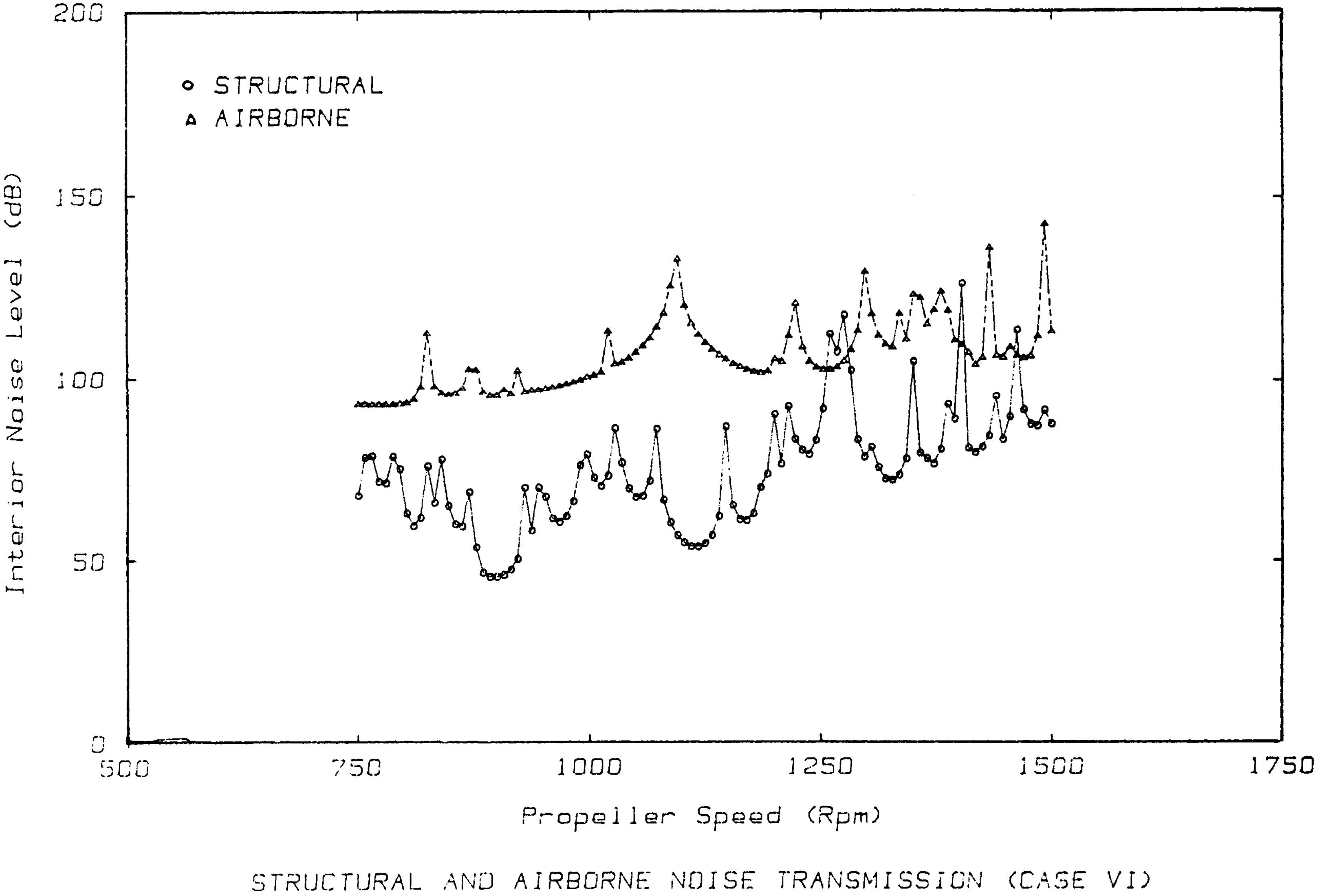

Figure 14. Interior noise levels for the structural model of Case VI.

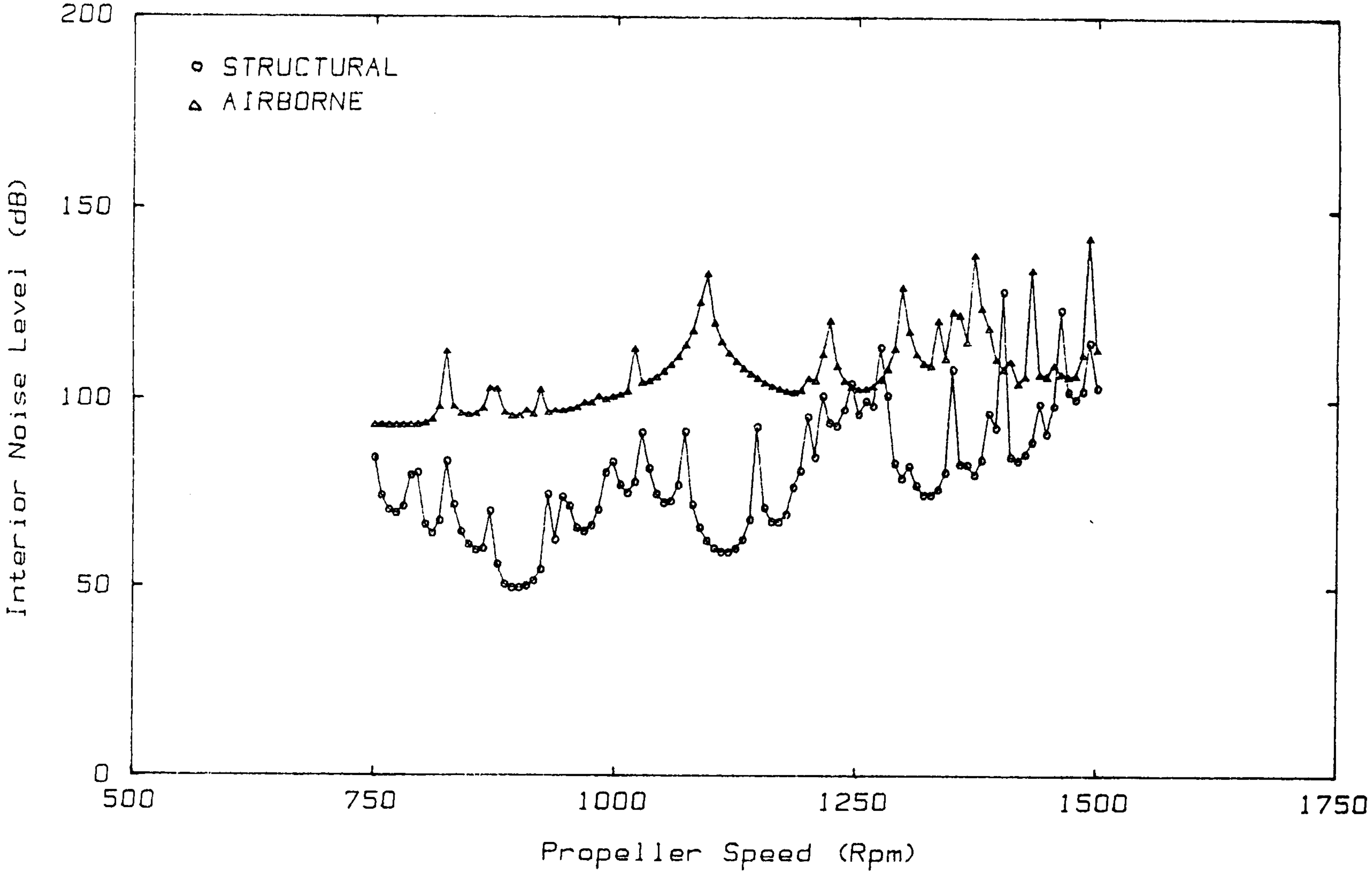

STRUCTURAL AND AIRBORNE NOISE TRANSMISSION (CASE VII)

Figure 15. Interior noise levels for the structural model of Case VII.

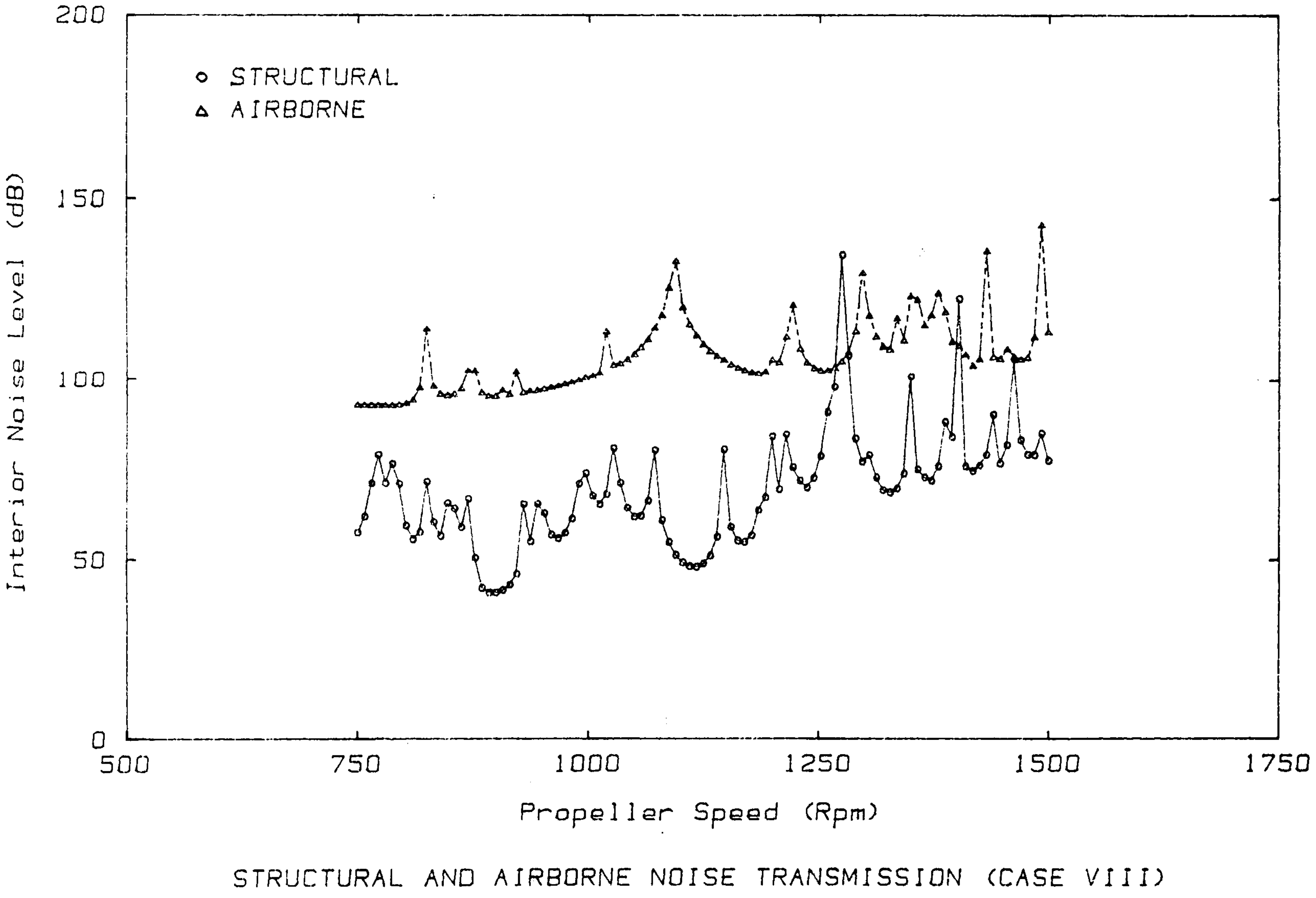

Figure 16. Interior noise levels for the structural model of Case VIII.

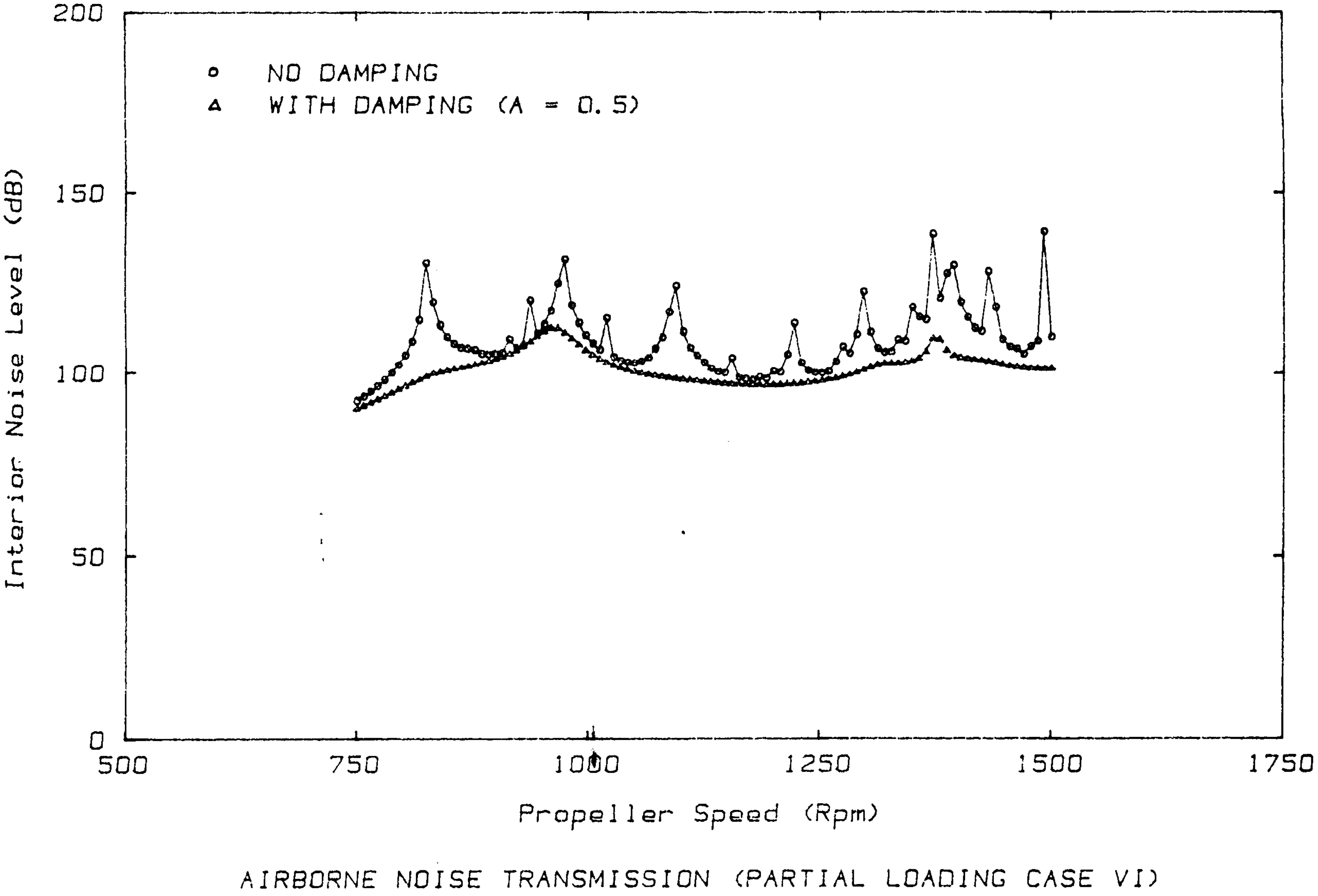

Figure 17. Interior noise level due to airborne transmission, partial loading for Case VI.

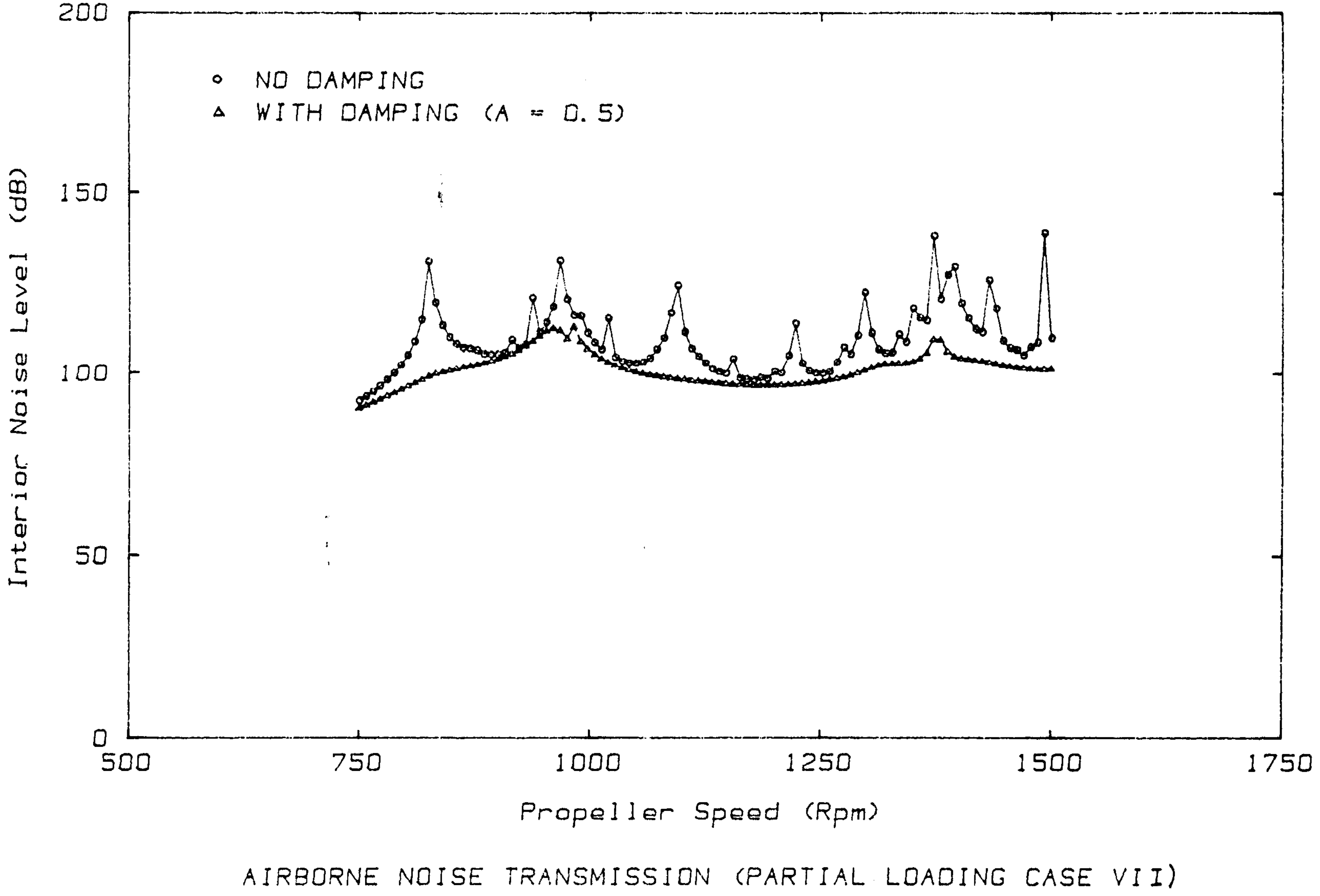

Figure 18. Interior noise level due to airborne transmission, partial loading for Case VII.

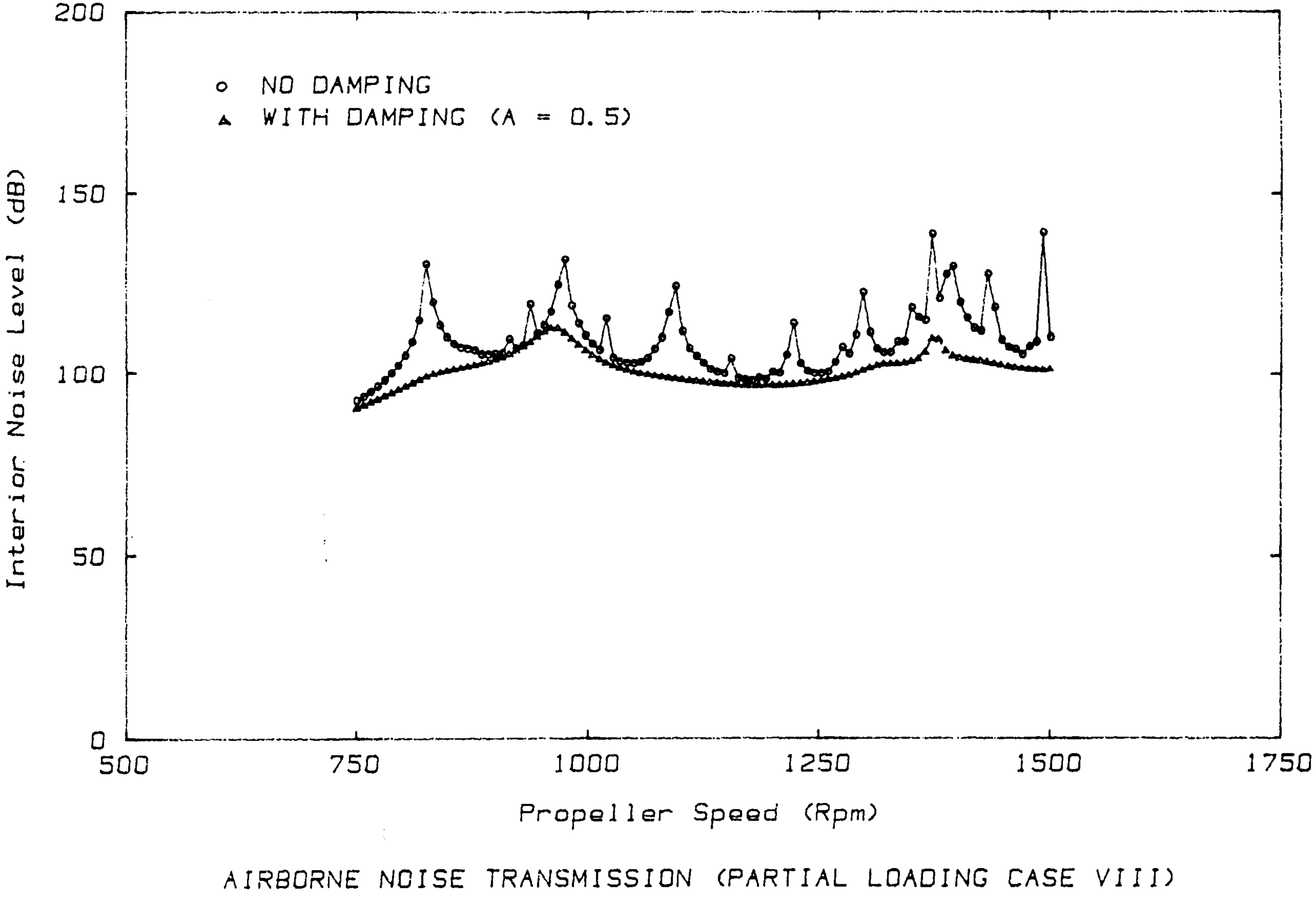

Figure 19. Interior noise level due to airborne transmission, partial loading for Case VIII.

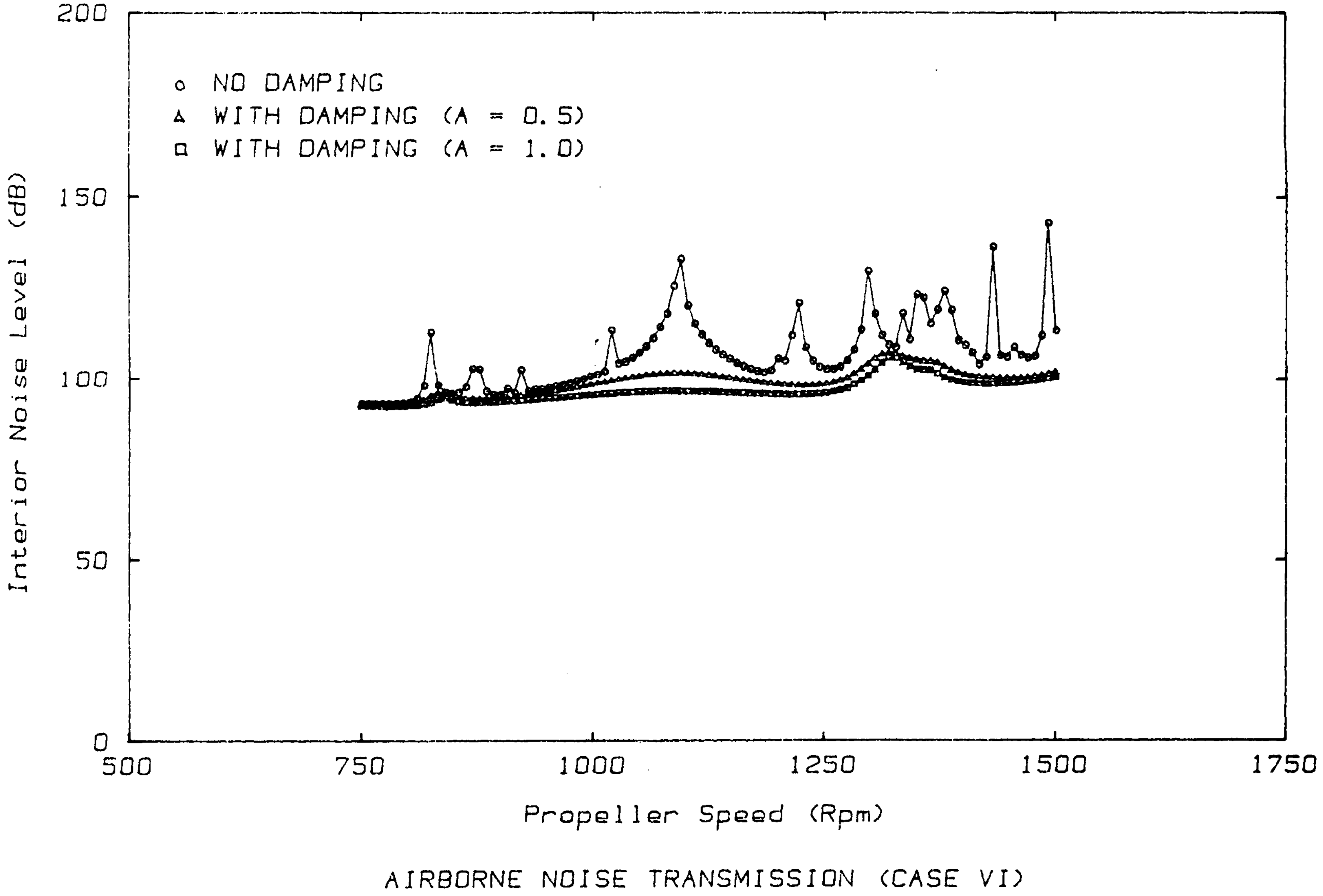

AIRBORNE NOISE TRANSMISSION (CASE VI)

Figure 20. Effect of interior absorption on interior noise levels due to airborne noise transmission for Case VI.

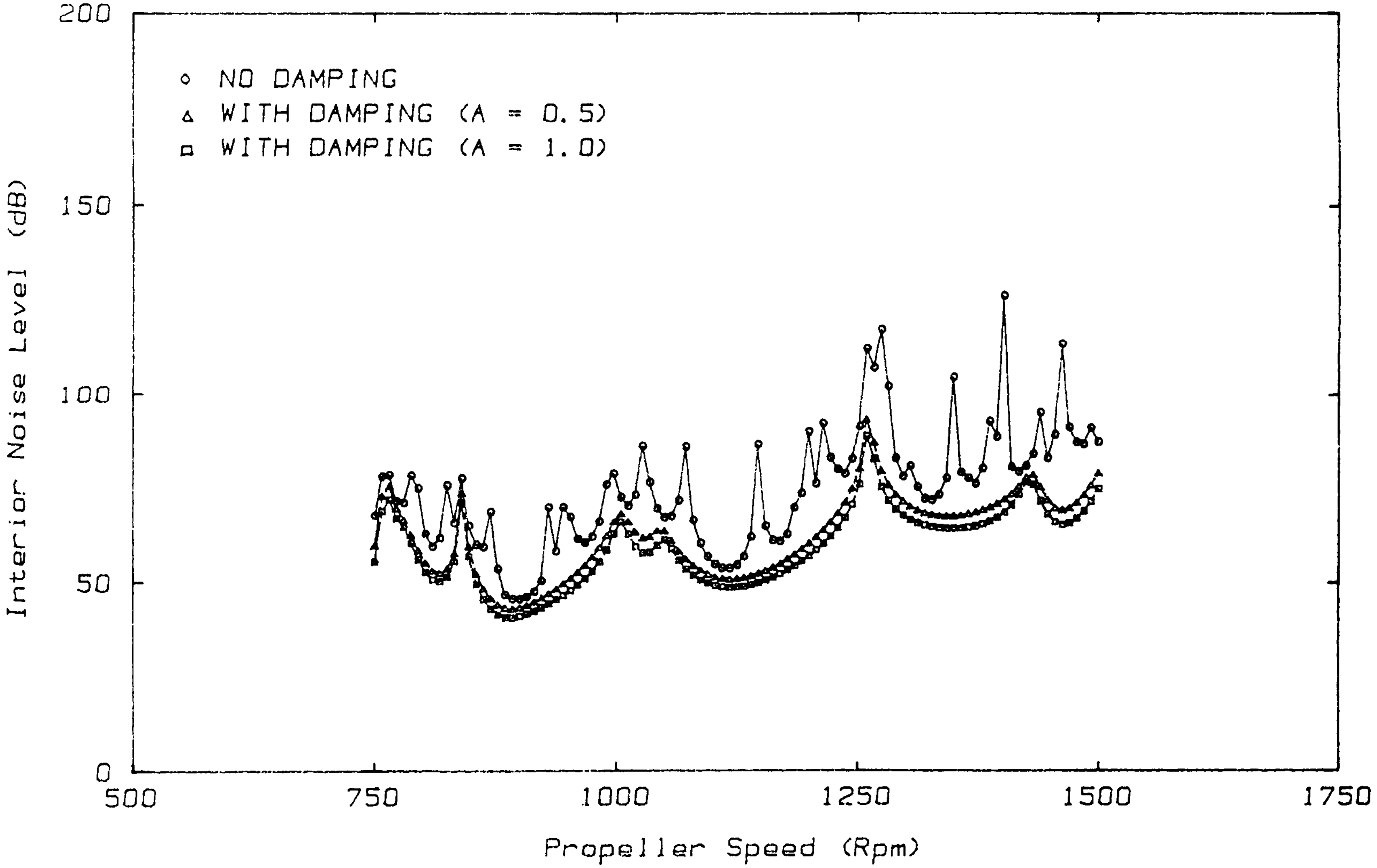

STRUCTURAL NOISE TRANSMISSION (CASE VI)

Figure 21. Effect of interior absorption on interior noise levels due to structureborne noise transmission for Case VI.

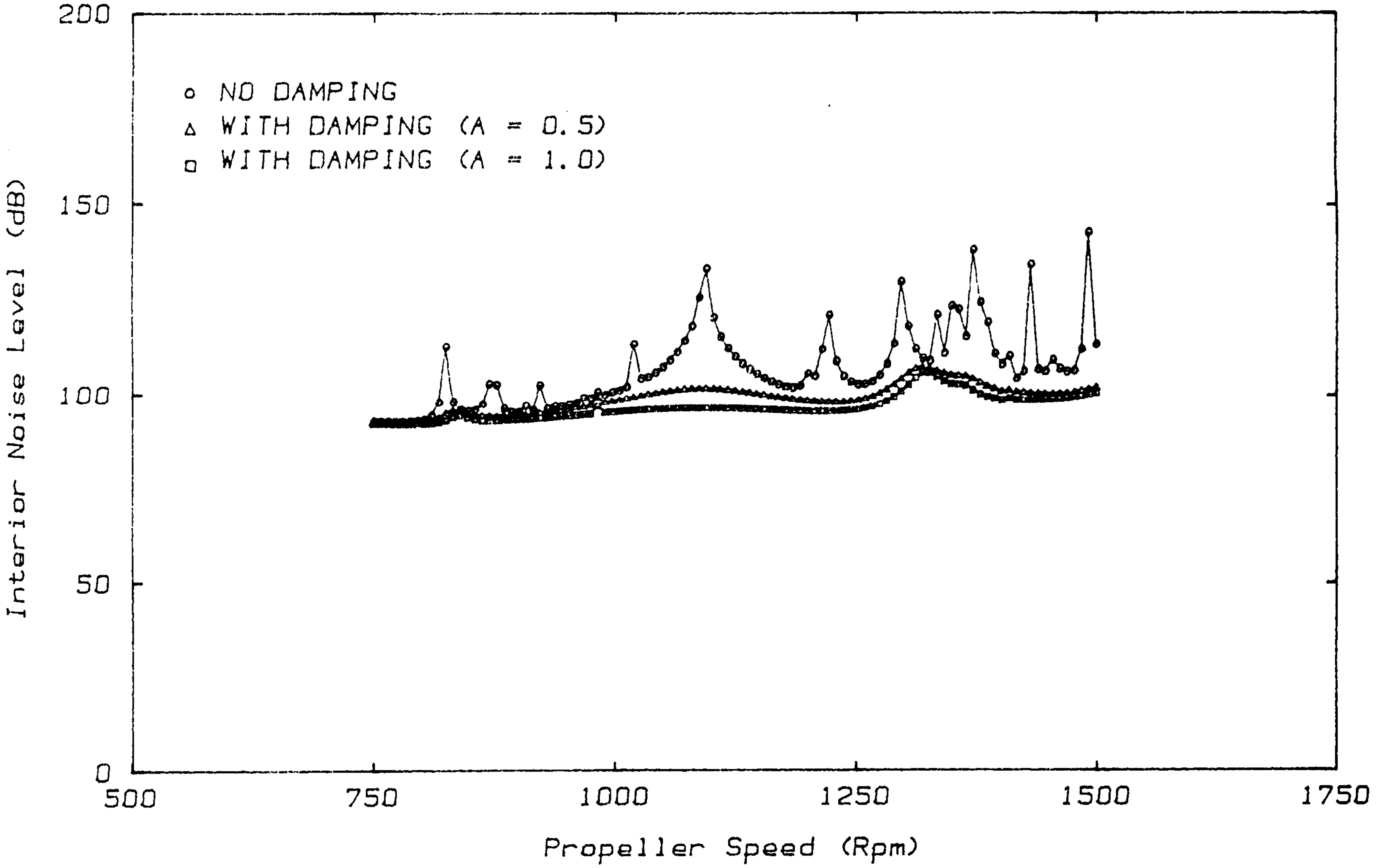

AIRBORNE NOISE TRANSMISSION (CASE VII)

Figure 22. Effect of interior absorption on interior noise levels due to airborne noise transmission for Case VII.

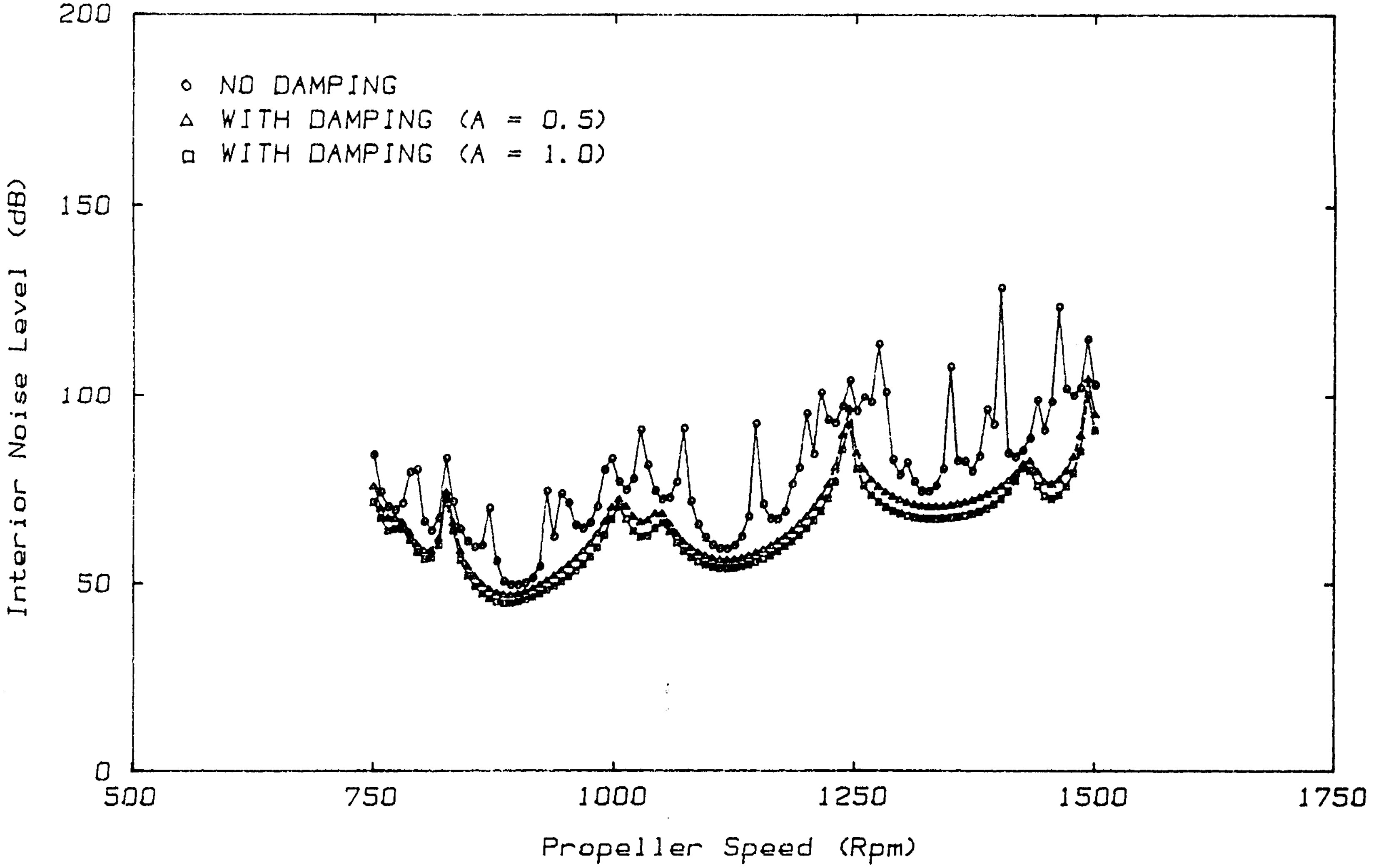

STRUCTURAL NOISE TRANSMISSION (CASE VII)

Figure 23. Effect of interior absorption on interior noise levels due to structureborne noise transmission for Case VII.

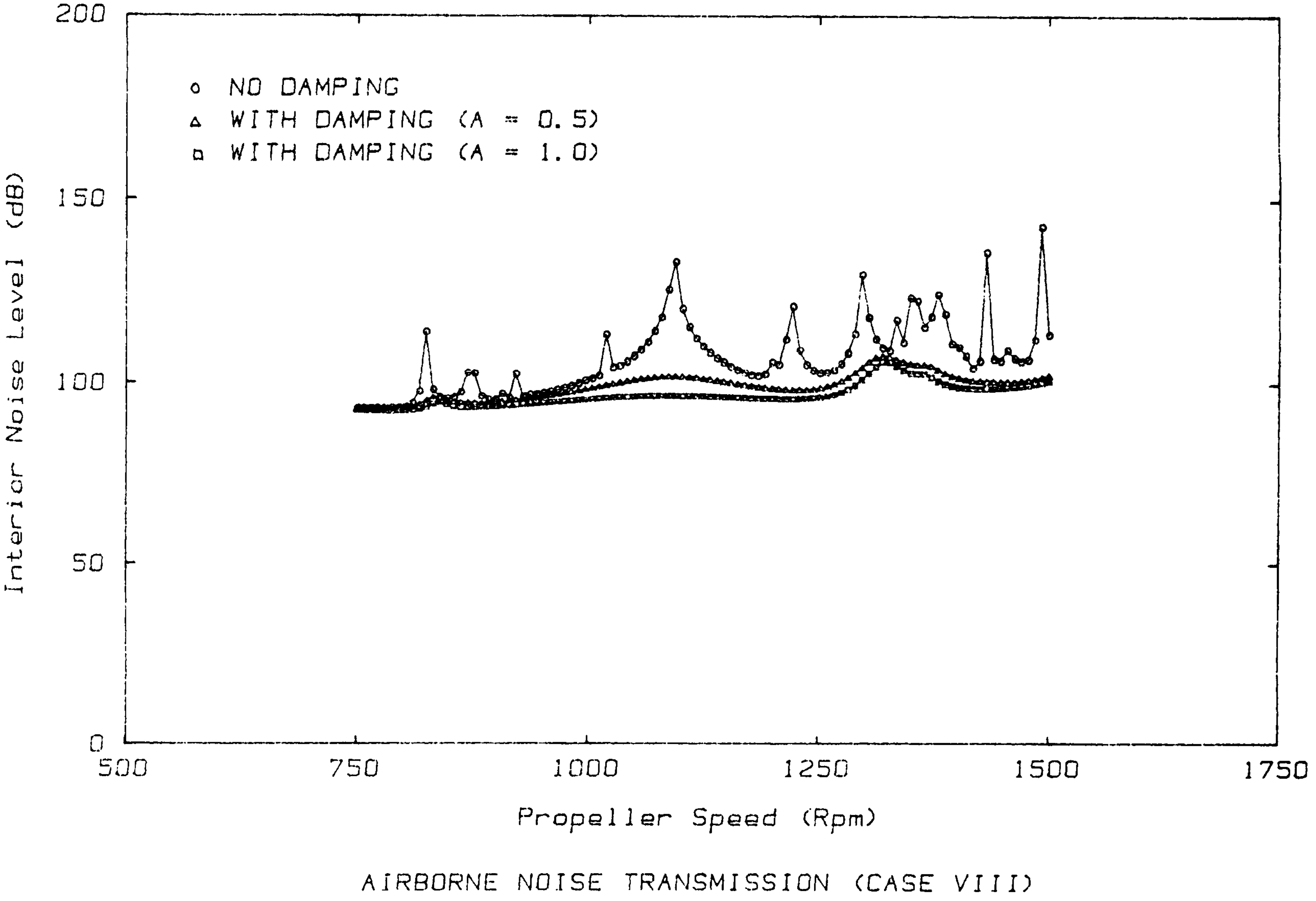

Figure 24. Effect of interior absorption on interior noise levels due to airborne noise transmission for Case VIII.

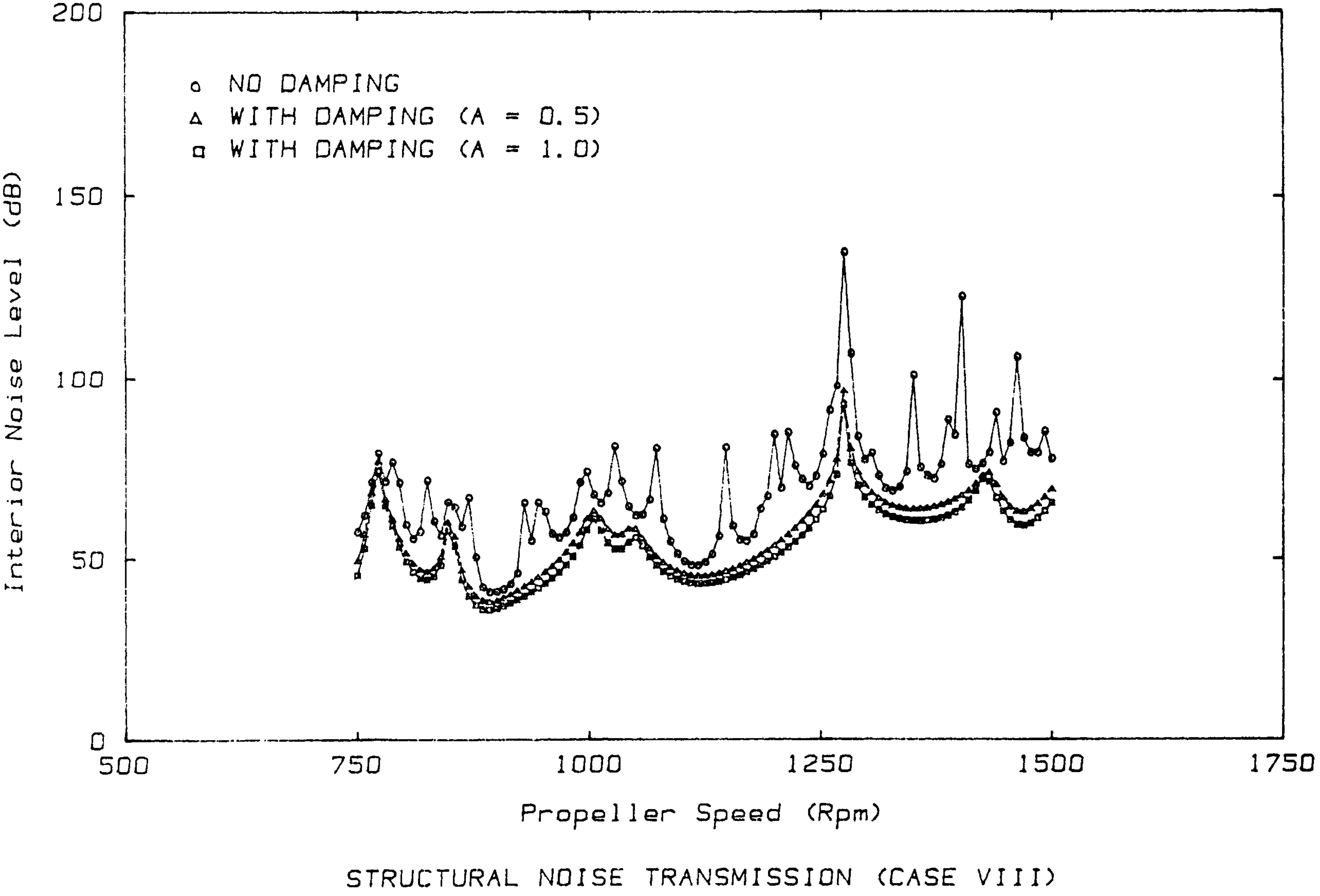

Figure 25. Effect of interior absorption on interior noise levels due to structureborne noise transmission for Case VIII.